ADVANCED ENERGY MATERIALS
www.advenergymat.de

Recent Advances in Emerging Non-Lithium Metal–Sulfur Batteries: A Review

Lianbo Ma, Yaohui Lv, Junxiong Wu, Yuming Chen,* and Zhong Jin**

Rechargeable non-lithium metal–sulfur batteries (MSBs) have gained tremendous attention because of their merits, including a high theoretical capacity, remarkable energy density, and low cost. However, the detrimental issues encountered by non-lithium MSBs, such as polysulfide shuttle effects, volume expansion and the low electrical conductivity of elemental sulfur, and the serious side reactions between metal anodes and electrolytes, severely restrict their practical applications. To circumvent these issues, numerous effective strategies have been explored and utilized. In this review, the intractable obstacles that prevent the application of non-lithium MSBs are first summarized. Recent pioneering studies on rechargeable non-lithium MSBs are reported and discussed in terms of material design, fabrication methods, and electrochemical performance. The emerging characterization techniques used to reveal the working mechanisms of non-lithium MSBs and the advantages of elaborately designed structures are highlighted. Finally, the remaining issues and possible future areas of research for practical applications are discussed.

1. Introduction

The rapid development of electronic markets has stimulated the exploration of new energy storage and conversion systems. Lithium-ion batteries (LIBs) are vital components, powering consumer electronics (e.g., mobile phones and laptops), electric vehicles (EVs), and energy storage units.[1–4] However, state-of-the-art LIBs are approaching their specific energy limits, and they cannot meet the ever-increasing energy demand, especially for EVs.[5,6] Therefore, the development of new energy storage and conversion devices is urgently required. Lithium–sulfur (Li–S) batteries are a major focus of academic and industrial energy storage research owing to their high theoretical capacity, high energy density, and low cost.[7–10] However, Li–S batteries normally suffer from several inherent disadvantages, including low electronic conductivity of sulfur and polysulfide intermediates, the polysulfide dissolution and shuttle effect, elemental sulfur volume expansion during charge/discharge processes, and formidable side reactions originated from Li metal anode and organic liquid electrolytes.[11–13] Various strategies including the exploration of micro- and nanostructured sulfur hosts, optimization of electrolyte formulas, modification of separators, and modulation of Li metal anodes have been developed to address these challenging issues. Apart from the safety concerns caused by the direct utilization of Li metal, the limited reserves and high cost of Li resources also impede the commercialization of Li–S batteries.[14–16]

As mentioned above, the anticipation of the increasing price and limited availability of Li has become a strong driving force for the exploration of other alkali and alkaline earth metals.[4,17,18] Non-lithium metal–sulfur batteries (MSBs) fabricated by coupling naturally abundant and environmentally friendly sulfur cathode with other metal anodes have attracted extensive interest, because of the similar electrochemical conversion reactions.[19] For example, sodium (Na) and potassium (K) have been employed because they locate the same group right below Li in the periodic table, thus sharing similar physical and chemical properties.[20–23] In addition, multivalent metallic anodes such as magnesium (Mg), calcium (Ca), and aluminum (Al) have also been explored because the resulting MSBs have even higher volumetric energy densities, as compared with Li–S batteries (**Figure 1**).[24,25] These non-lithium MSBs experience similar issues to Li–S batteries; therefore,

Dr. L. Ma, Prof. Y. Lv
Key Laboratory of Green Fabrication and Surface Technology of Advanced Metal Materials
Ministry of Education
Anhui University of Technology
Maanshan 243002, China
Dr. L. Ma, Prof. Z. Jin
Key Laboratory of Mesoscopic Chemistry of MOE
Jiangsu Key Laboratory of Advanced Organic Materials
State Key Laboratory of Coordination Chemistry
School of Chemistry and Chemical Engineering
Nanjing University
Nanjing 210023, China
E-mail: zhongjin@nju.edu.cn
Dr. L. Ma, Prof. Z. Jin
Shenzhen Research Institute of Nanjing University
Shenzhen 518063, China
Dr. J. Wu
Department of Mechanical Engineering
The Hong Kong Polytechnic University
Kowloon, Hong Kong, China
E-mail: jwuba@connect.ust.hk
Prof. Y. Chen
College of Environmental Science and Engineering
Fujian Normal University
Fuzhou 350007, China
E-mail: yumingc126@126.com
The ORCID identification number(s) for the author(s) of this article can be found under https://doi.org/10.1002/aenm.202100770.

DOI: 10.1002/aenm.202100770

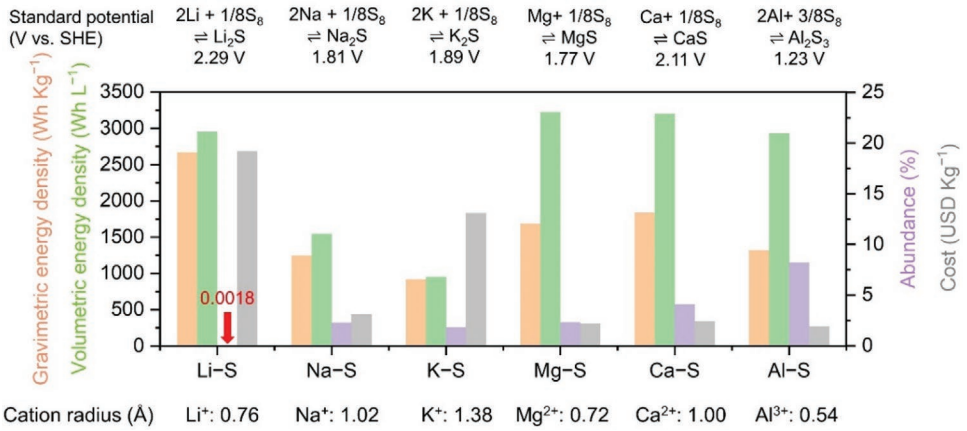

Figure 1. Parameter comparisons of Li atoms with other metal atoms and those of the corresponding Li–S batteries with those of other non-lithium MSBs.

solutions and strategies adopted in Li–S batteries can be transferred to non-lithium MSBs, which accelerates the development of non-lithium MSBs. Notably, there are also some differences between Li–S batteries and other non-lithium MSBs. For instance, Na and K metals are more chemically active than Li,[26,27] thus requiring stricter conditions, whereas the sluggish kinetics of multivalent Mg^{2+} and Ca^{2+} cations are responsible for the relatively poorer electrochemical performance of Mg–S and Ca–S batteries.[28] As such, these newly emerged MSBs encounter even more severe and complicated problems, which must be solved for commercialization.

To completely address the above-mentioned issues faced by non-lithium MSBs, various strategies have been proposed, including the rational design of micro- and nanostructured cathodes, optimization of the electrolyte formula, and modification of separators. It has been recently confirmed that these strategies are effective for non-lithium MSBs. For instance, carbonaceous materials with various micro- nanostructures have been designed and constructed as sulfur hosts for non-lithium MSBs, thus resulting in good electrochemical performance.[29] In addition, myriads of efforts have been devoted to the exploration of new electrolytes,[30–33] modulation of metal anodes,[34–36] and modification of separators.[37–39] Strategies to mitigate the issues faced by metal anodes have been extensively reviewed, and as such, this review will refrain from reiterating this aspect of the field.

In this review, we first summarize the challenges encountered with non-lithium MSBs and discuss their formation processes in-depth. We then move on to the recently employed strategies to resolve the challenging issues associated with various non-lithium MSBs. Special focus is placed on the fundamental understanding of their structure-composition-performance relationships. Additionally, state-of-the-art characterization techniques are highlighted to help understand the working mechanisms of non-lithium MSBs. Finally, the remaining issues and perspectives of non-lithium MSBs are given and discussed.

2. Challenges of Non-Lithium MSBs

Non-lithium MSBs suffer from several notorious issues similar to Li–S batteries, such as the insulating nature of elemental sulfur and polysulfides, severe volume changes of sulfur, shuttling effect of metal polysulfides, and unstable metal anodes, as illustrated in **Figure 2**.

(i) **Insulating nature of elemental sulfur**. In most MSBs, elemental sulfur is directly used as the cathode material, with fresh metals serving as anodes. However, the insulating nature of elemental sulfur leads to sluggish charge transfer and electrochemical reaction kinetics, causing severe battery polarization, especially at high current rates.[40–42] A combination of highly conductive materials with sulfur has proven to be effective in circumventing this issue. Thus, various carbonaceous matrices (e.g., graphene, carbon nanotubes (CNTs)), MXenes, and conductive polymers have been used to construct sulfur composites for high-performance sulfur cathodes.[43–45]

(ii) **Severe volume changes in sulfur during the charge/discharge cycles**. The mass density of elemental sulfur is ≈2.07 g cm^{-3}, while the generated polysulfides have a relatively lower density, for example, the mass density of sodium sulfide decreases to 1.86 g cm^{-3}.[46] Thus, elemental sulfur undergoes an obvious volume expansion during electrochemical cycles, leading to dramatic structural damage of sulfur cathodes and a short lifespan of MSBs. To this end, the rational design of sulfur cathodes with sufficient space is essential to alleviate the volume changes of elemental sulfur.

(iii) **Dissolution and shuttle effects of polysulfides**. Similar to Li–S batteries, non-lithium MSBs experience serious shuttle effects on metal polysulfides.[47,48] During the discharge process, metal cations diffuse into the sulfur cathode region and react with sulfur, forming a series of metal polysulfides. However, the initially generated polysulfides are highly soluble in ether-based electrolytes; therefore, the dissolved metal polysulfides passivate metal anodes because of the force driving the concentration gradient and the high reactivity of metals. As such, not only is active sulfur consumed but the anode is also passivated, which results in fast capacity fading in MSBs. Physical restriction and chemical confinement are two well-known strategies for resolving the shuttling of polysulfides. Physical restriction relies on the design of meso/macropores which trap metal polysulfides by physical absorption or by

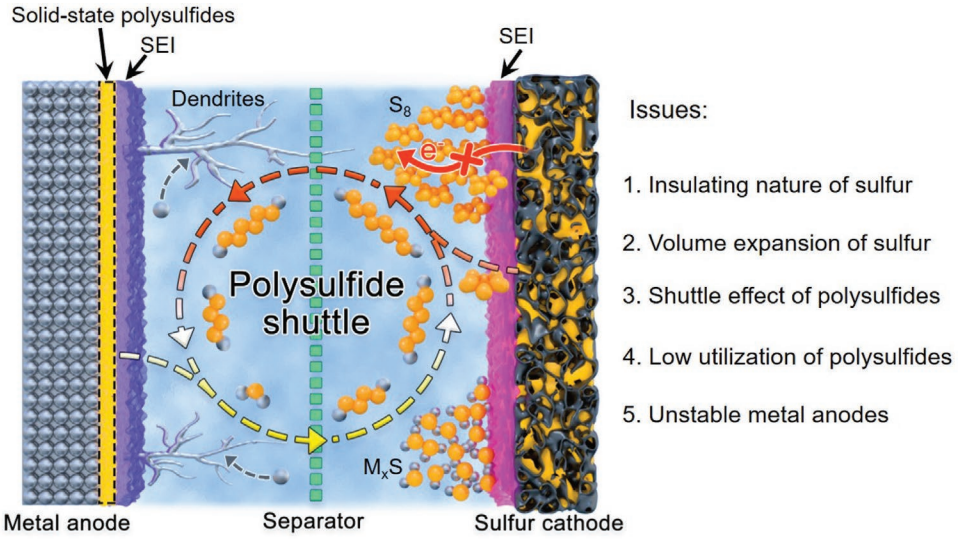

Figure 2. Schematic illustration of the pressing challenges of non-lithium MSBs.

molecularly confining sulfur in the micropores, while chemical confinement immobilizes the polysulfides through chemical bonds formed between the functional species and soluble polysulfides, thus alleviating their dissolution and diffusion in the electrolytes. Recently, the integration of two strategies has become more popular because the synergistic effect can further reduce the loss of active sulfur.

(iv) **Low conductivity and low utilization of intermediate polysulfides**. Metal polysulfides are normally produced during discharge and possess low electrical conductivities.[49,50] The low electrical conductivity of active materials inevitably impedes the electrochemical redox reactions, thus degrading the utilization of intermediate polysulfides. Moreover, long-chain polysulfides tend to dissolve in the electrolyte and shuttle between the cathode and anode, resulting in a significant loss of active species.

(v) **Unstable non-lithium metal anodes**. In MSBs, the metal anodes are directly exposed to electrolyte solutions and undesired side reactions may occur because of their high reactivity. Metal anodes exhibit large volume expansion during plating processes, causing the cracking of solid-electrolyte interphase (SEI) layers and low Coulombic efficiency (CE). Furthermore, the uneven distribution of ion flux intensifies the non-uniform nucleation and growth of metal dendrites, which may evolve into inactive species upon repeated cycles.[51,52] In addition, the capacity of the anode and cathode should be well-matched to maximize the energy density of the MSBs, which means that the amount of metal anode should be carefully controlled. Therefore, a highly reversible metal plating/stripping efficiency is required to prolong the cycle life of MSBs. Substantial efforts have been devoted to addressing the unstable properties of metal anodes, including the construction of novel anode structures, the modification of separators, optimization of electrolyte formulations, and application of protective layers on metal anode surfaces, which have been referred to in some excellent reviews.[51,52]

(vi) **Differences between non-lithium MSBs and Li–S batteries**. Despite their similarities, non-lithium MSBs also exhibit some intrinsic differences. For example, K ions have a much larger radius than Li-ions, resulting in sluggish reaction kinetics with a final discharge product, K_xS ($x < 2$). It has been reported that the final discharge product is in the range of $KS_{0.67–0.85}$.[53] In the case of multivalent MSBs, elemental sulfur experiences an even larger volume expansion (up to 272%) upon complete discharge.[39] Moreover, multivalent metal ions are commonly incompatible with organic electrolyte solutions; thus, new electrolyte systems must be explored and developed to accelerate metal ion transfer and reversible platting/stripping of metal anodes. The working principles of non-lithium MSBs are yet to be clarified. Although various strategies have been adopted aiming at enhancing electrochemical performance, a fundamental understanding of the reaction mechanism is required.

3. Na–S Batteries

Na–S batteries have caused tremendous interest owing to their electrochemical result, including high energy density and low Na and sulfur costs.[54] In the 1960s, high-temperature operated Na–S batteries emerged with molten Na as the anode and sulfur as the cathode.[55] However, the working temperature (above 300 °C) is relatively high, which causes safety concerns and high operation costs.[56] With the development of new electrolytes, room-temperature (RT) Na–S redox reactions can occur, widening the application of Na–S batteries. In the following section, we discuss recent advances in Na–S batteries from the aspects of cathode construction, electrolyte optimization, and separator modification.

3.1. Cathodes for Na–S Batteries

The architecture of the cathodes determines directly the achieved electrochemical performance of Na–S batteries. Based on different sulfur cathodes, the discussions here are divided

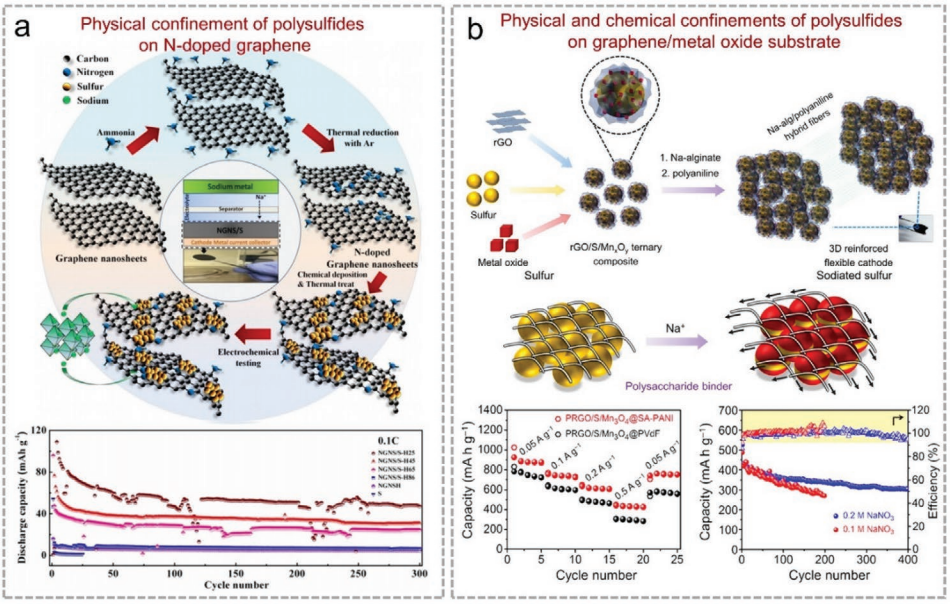

Figure 3. a) A schematic illustration and electrochemical tests of N-doped graphene nanosheets/sulfur nanocomposites as the cathode material in Na–S batteries and long-term cyclic performance of various cathodes at 0.1 C. Reproduced with permission.[59] Copyright 2017, Wiley-VCH. b) Schematic illustration of the synthesis of a freestanding cathode and the role of binder, as well as the electrochemical performance of the cathode. Reproduced with permission.[60] Copyright 2019, American Chemical Society.

into carbon-based and other sulfur composite cathodes, sodium sulfide and polysulfide cathodes, covalent polymer-sulfur cathodes, and metal sulfide cathodes.

3.1.1. Carbon/Sulfur and Other Sulfur Composite Cathodes

Graphene and Reduced Graphene Oxide (RGO)-based Sulfur Hosts: Owing to their high electrical conductivity, excellent structural and electrochemical stability, and tunable pore structures, nanocarbons have been widely employed as sulfur hosts for Na–S batteries. Among the various nanocarbons, graphene, a 2D material with atomic thickness, has been explored for the fabrication of sulfur cathodes.[57,58] For instance, nitrogen (N)-doped graphene has been reported as a sulfur host (**Figure 3**a).[59] Benefiting from the improved kinetics originating from the highly conductive N-doped graphene networks, sulfur nanocomposites were found to exhibit good electrochemical performance (specific capacity of 136 mAh g^{-1} at the 10th cycle under 0.05 C) with an electrolyte/sulfur (E/S) of 50 µL mg^{-1}. To mitigate the dissolution of polysulfides, Mitra et al. applied RGO as a sulfur host because the oxygen-containing functional groups on the surfaces of RGO provide abundant active sites for the adsorption of polysulfide molecules. They further integrated RGO with valence manganese oxides and sulfur particles to fabricate a sulfur cathode. With the help of a hybrid Na alginate/polyaniline binder, the polysulfide shuttle effect was restricted, and a high CE of above 99% was maintained for 100 cycles with an E/S of ≈20 µL mg^{-1}, as shown in Figure 3b.[60] Such a design concept allows the homogeneous distribution and maximum utilization of elemental sulfur in electrochemical redox reactions.

Carbon Fibers as Sulfur Hosts: Carbon fibers have also attracted tremendous attention because of their conductive and interconnected networks, as well as their high electrolyte adsorption capability.[61,62] Niu et al. fabricated a freestanding sulfur cathode by loading sulfur on carbon fiber (**Figure 4**a).[63] The carbon fiber/sulfur electrode with an areal loading of 2.0 mg cm^{-2} delivered a specific discharge capacity of ≈390 mAh g^{-1} at 0.1 C and good cyclic stability for 300 cycles with an E/S ratio of 10 mL g^{-1}. Xia et al. prepared electrospun carbon nanofiber/sulfur composites for all-solid-state Na–S batteries.[64] The as-obtained Na–S batteries displayed a high specific capacity of 252 mAh g^{-1} in the second cycle and maintained a capacity of 251 mAh g^{-1} after 100 cycles, accompanied by an average CE of ≈100%. To further promote the conversion kinetics of RT Na–S batteries, Se was introduced into the sulfur composites to enhance the electronic conductivity of the composite cathodes.[65] For example, Zeng et al. impregnated $S_{0.96}Se_{0.04}$ into flexible porous carbon nanofibers (PCNFs), serving as the electrode for RT Na–S batteries (Figure 4b). The pores in the carbon nanofibers enabled a high loading of S_xSe_{1-x} (≈72 wt%).[65] The $S_{0.96}Se_{0.04}$@PCNFs displayed excellent electrochemical result (specific capacity of 762 mAh g^{-1} calculated based on the mass of $S_{0.96}Se_{0.04}$ after 100 cycles at 0.1 A g^{-1}), which is much higher than that of S@PCNFs (309 mAh g^{-1}). Additionally, the hybrid cathodes exhibited an excellent rate capability of 181 mAh g^{-1} at 20 A g^{-1}. Similar results were obtained when $S_{0.6}Se_{0.4}$ was selected as the active component.[66]

Porous Carbon Material-Based Sulfur Hosts: Porous carbon architectures with large specific surface areas and abundant pores are promising hosts for Na–S batteries.[67–72] The large specific surface area and high pore volume not only ensure a high sulfur content in the composite cathodes but also alleviate the volume changes of sulfur. In addition, the high electrical

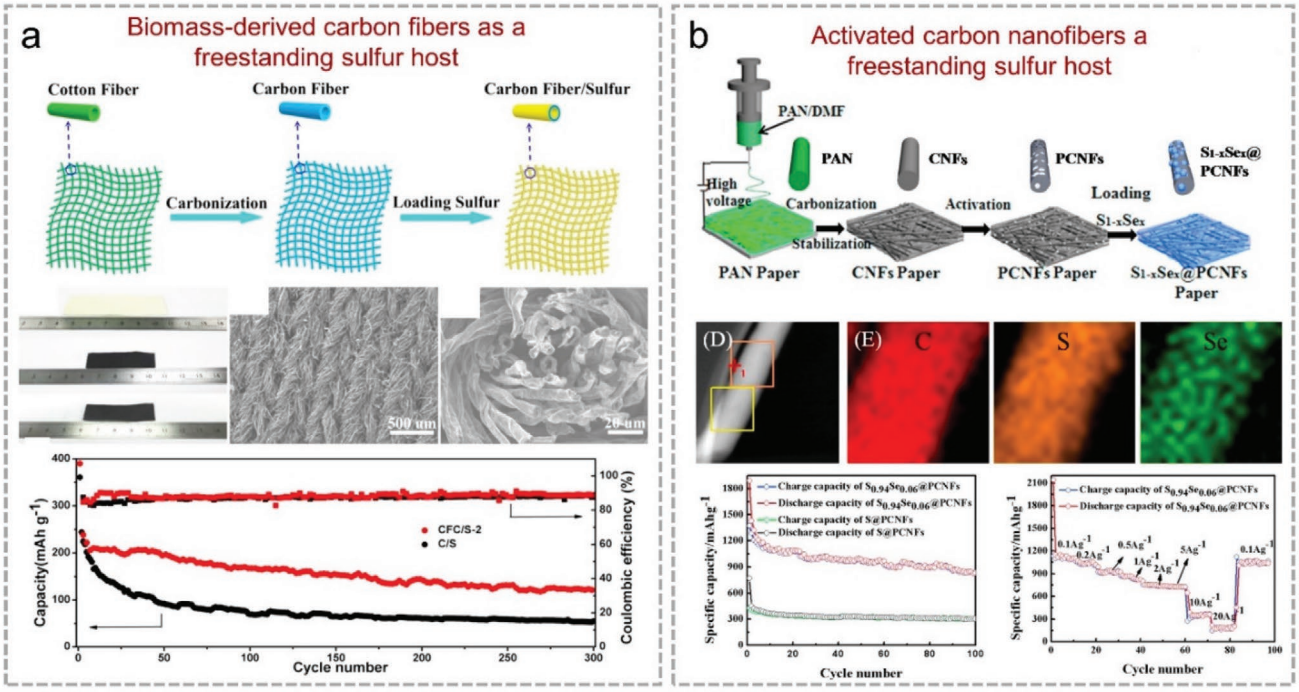

Figure 4. a) Schematic illustration and morphology of sulfur composites and their long-term cyclic performance. Reproduced with permission.[63] Copyright 2017, Elsevier. b) Schematic illustration, elemental maps, and electrochemical performance of sulfur cathodes. Reproduced with permission.[65] Copyright 2016, Elsevier.

conductivity of porous carbon provides fast electron transfer during electrochemical reactions.[67] Metal–organic frameworks (MOFs) are typical precursors for the production of porous carbon materials. Rogach et al. reported a MOF-derived S, N co-doped porous carbon skeleton with 3D tubular holes for Na–S batteries (**Figure 5**a).[72] Using a vapor-infiltration method, sulfur species were bonded with the carbon structures; this method is different from the commonly employed melt-diffusion method to physically confine sulfur species. The sulfur cathodes demonstrated outstanding electrochemical performance with high capacities (467 mAh g^{-1} at 0.1 A g^{-1}, 270 mAh g^{-1} after 1000 cycles at 1.0 A g^{-1}) and excellent rate capability (304 mAh g^{-1} at 10 A g^{-1}). Mesoporous N-doped carbon nanospheres prepared by thermal annealing of Fe^{3+}/polyacrylamide nanospheres were used as the sulfur matrix.[69] The N-doped carbon nanospheres not only blocked the shuttle effects of sodium polysulfides but also improved the utilization of active sulfur species. Thus, the S@N-doped carbon nanospheres maintained a high capacity of 639 mAh g^{-1} after 400 cycles at 0.1 C and excellent cyclic stability for 800 cycles at 0.5 C (Figure 5b).

In addition to the commercial porous carbon materials,[73,74] other porous carbon matrices prepared through the template method,[75–79] direct carbonization of biomass and organic complexes,[80–84] and wet-chemical synthesis approaches[85] have also been employed as sulfur hosts for RT Na–S batteries. Chou et al. constructed an elaborately designed carbon framework, called interconnected mesoporous hollow carbon nanosphere, as a sulfur host for RT Na–S batteries (**Figure 6**a).[75] In situ X-ray diffraction (XRD) patterns revealed that the carbon framework suppressed the dissolution of sodium polysulfides and enabled reversible reactions between S_8 molecules and Na_2S_4. Consequently, the sulfur cathode retained ≈88.8% of its initial capacity after 200 cycles and exhibited a superior rate capability (127 mAh g^{-1} at 5.0 A g^{-1}). Recently, coffee residues were carbonized to obtain porous carbon with abundant ultramicropores, which were then used as the sulfur host.[81] Both theoretical simulations and experimental results confirmed that no soluble Na_2S_n ($2 \le n \le 8$) was generated and Na_2S was the final discharge product because of the restricted interlayer distance of the biomass-derived carbon matrix. The sulfur/carbon composite exhibited an ultrahigh specific capacity of 1492 mAh g^{-1} at 0.1 C and excellent cyclability over 2000 cycles without any capacity decay (Figure 6b). In addition, Jiang et al. applied an in situ wet-chemical solvothermal method to construct carbon nanostructures to enhance the adsorption of sulfur molecules.[85] The as-fabricated sulfur cathode presented extremely high specific capacities of 889 and 811 mAh g^{-1} after 600 cycles and 950 cycles at 0.8 and 1.6 C, respectively, and exceptional rate performance (700 mAh g^{-1} at 8.1 C), demonstrating great potential for practical RT Na–S batteries.

Constructing carbon architectures comprising various carbon matrices can take advantage of each component to synergistically prevent the shuttle effect of soluble polysulfides and enhance the electrochemical performance of Na–S batteries.[86,87] Guo et al. pioneered the development of microporous carbon for RT Na–S batteries. A coaxial cable-like structure with a CNT inside a microporous carbon sheath was fabricated, where the inner CNTs served as the electrically conductive channels for promoting fast electron transfer, and the mesoporous

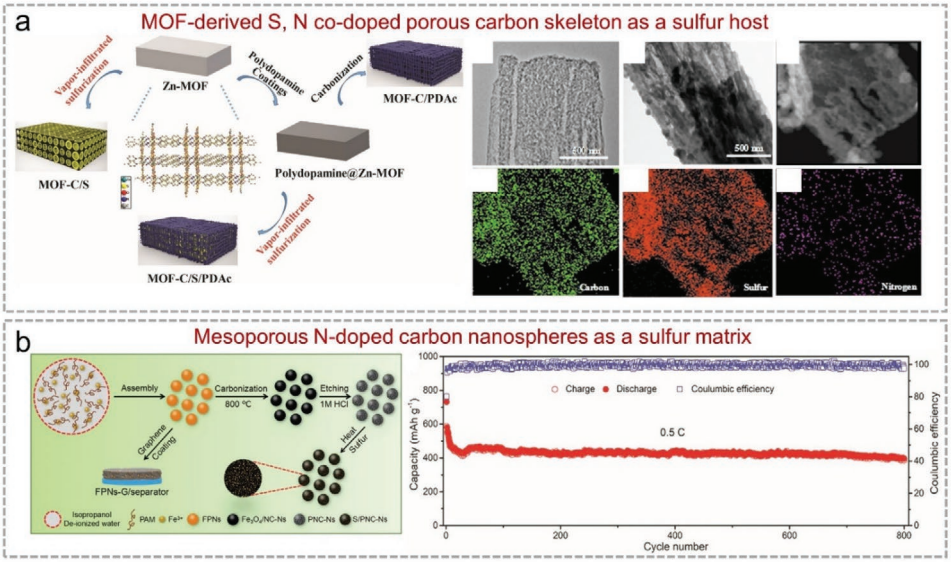

Figure 5. a) Synthesis procedure and structure of S, N co-doped porous carbon as the sulfur hosts of Na–S batteries. Reproduced with permission.[72] Copyright 2020, Wiley-VCH. b) Schematic illustration of the synthesis of N-doped carbon spheres and the electrochemical performance of N-doped carbon spheres as the sulfur host for Na–S batteries. Reproduced with permission.[69] Copyright 2020, Wiley-VCH.

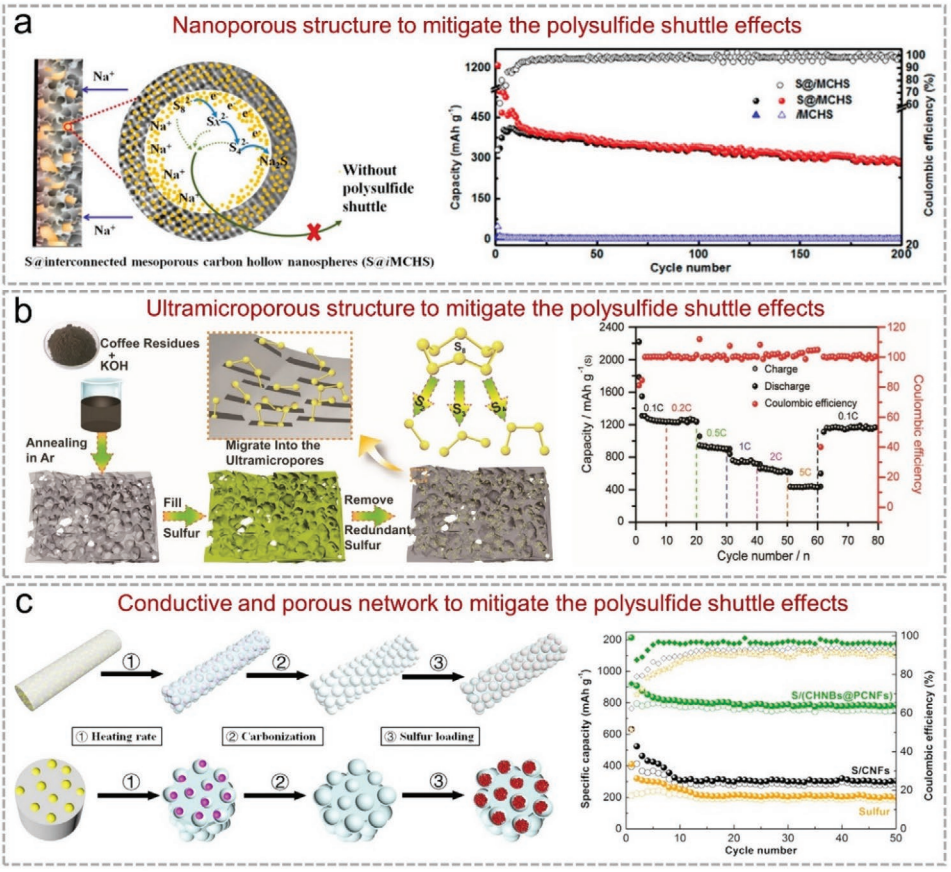

Figure 6. a) Schematic illustration and electrochemical performance of S@interconnected mesoporous carbon hollow nanospheres as the sulfur hosts of Na–S batteries. Reproduced with permission.[75] Copyright 2016, American Chemical Society. b) Synthesis procedures and electrochemical results of sulfur confined in ultramicroporous carbon architectures as the sulfur hosts of Na–S batteries. Reproduced with permission.[81] Copyright 2020, Wiley-VCH. c) Synthesis and electrochemical performance of S@CHNB composite for Na–S batteries. Reproduced with permission.[87] Copyright 2018, Elsevier.

carbon sheath acted as the loading site for sulfur.[86] The as-obtained RT Na–S batteries displayed a long life of 200 cycles and a high specific energy density of 955 Wh kg^{-1}. Yu et al. precisely controlled the preparation of hollow carbon nanobubbles on porous carbon nanofibers (CHNBs@PCNFs) by electrospinning.[87] The heteroatom-doped CHNBs@PCNFs showed high electrical conductivity and strong adsorption ability to sodium polysulfides. The resulting sulfur/carbon cathodes exhibited a high reversible capacity of 256 mAh g^{-1} at 2.0 C (Figure 6c).

Hybrid Carbon Composite-Based Sulfur Hosts: Although different carbon materials have been explored to alleviate the dissolution of polysulfides, the non-polar carbon matrix can only trap polysulfides through physical interactions. In contrast, metal and metal compounds show high chemical adsorption capabilities with intermediate polysulfides.[88–90] Therefore, a more reasonable approach is to design hybrid hosts that combine highly conductive carbonaceous materials with highly polar compounds such as metals,[91–95] metal oxides,[96,97] metal sulfides,[98–102] metal carbides,[103,104] metal phosphides,[105] and metal oxyhydroxides.[106] Taking molybdenum disulfide (MoS_2) as a typical example; Xu et al. prepared a sulfur carrier of hollow carbon spheres decorated with MoS_2 nanosheets (**Figure 7**a).[98] The hollow carbon spheres can serve as a reservoir for sulfur species and electrolytes, whereas the outer MoS_2 nanosheets chemically absorb the soluble sodium polysulfides. Thus, the sulfur cathode displayed a high capacity of 1309 mAh g^{-1} at 0.1 C and excellent cyclic stability for 1000 cycles at 1.0 C. Moreover, Dou et al. constructed a multifunctional sulfur host composed of NiS_2 nanocrystals implanted into N-doped porous CNTs.[99] The sulfur host facilitated both physical confinement and chemical bonding of intermediate sodium polysulfides, thus effectively suppressing their dissolution and shuttle effects (Figure 7b). The highly reversible conversion reactions between soluble sodium polysulfides and insoluble Na_2S/Na_2S_2 are responsible for the excellent electrochemical performance.

Other Sulfur Hosts: Other materials, including MXene[107,108] and MOFs,[109,110] have also been employed to prepare sulfur cathodes for Na–S batteries. For example, Wang et al. prepared a 3D wrinkled MXene nanoarchitecture with a high specific surface area through a vacuum freeze-drying method (Figure 7c).[107] The MXene/S composite cathode effectively suppressed the dissolution and shuttle effect of sodium polysulfides and achieved good electrochemical performance (577 mAh g^{-1} after 500 cycles at 2.0 C) with a high sulfur

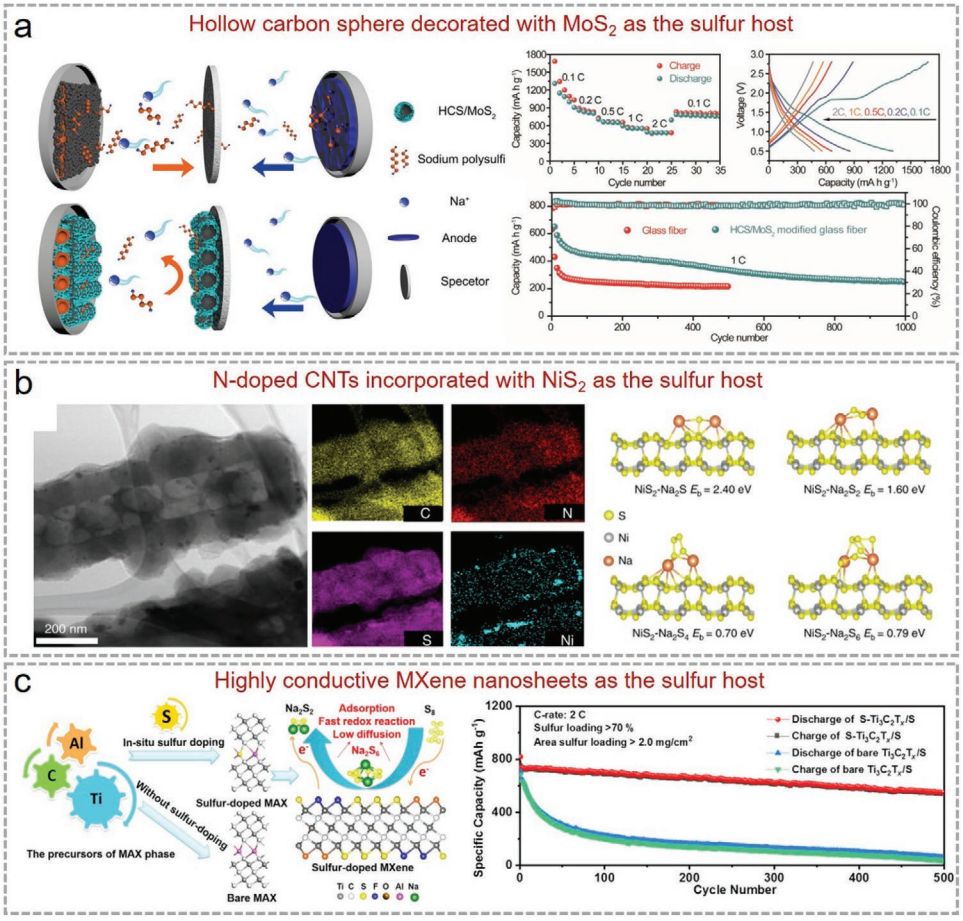

Figure 7. a) Schematic diagrams of S@HCS/MoS_2 serving as the cathode of Na–S batteries and its electrochemical performance. Reproduced with permission.[98] Copyright 2019, Wiley-VCH. b) Morphology and electrochemical performance of NiS_2 on N-doped porous CNTs serving as the sulfur cathode of Na–S batteries. Reproduced with permission.[99] Copyright 2019, Nature Publish Group. c) Schematic diagrams of the preparation of MXene/sulfur composite and its electrochemical performance for Na–S batteries. Reproduced with permission.[107] Copyright 2019, American Chemical Society.

loading (4.5 mg cm^{-2}). Moreover, Qiao et al. reported a 2D MOF to realize the chemical interactions between polysulfides and the Ni centers in MOFs, resulting in the strong adsorption and fast conversion kinetics of polysulfides.[109] Consequently, high specific capacities of 347 and 241 mAh g^{-1} were obtained with an E/S ratio of 20 µL mg^{-1} at 1.0 and 2.0 C after 1000 cycles, respectively, which are among the most stable electrochemical performances reported so far.

3.1.2. Sodium Sulfide and Polysulfide Cathodes

Sodium polysulfides (Na_2S_x) can also serve as active materials for Na–S batteries. The use of Na_2S_x avoids the incomplete utilization of active sulfur and further ensures high reversibility of Na–S batteries. Studies have extensively focused on taking advantage of the physical confinement concept to encapsulate sodium disulfides (Na_2S) into the voids and pores of carbonaceous materials.[111–116] Wang et al. embedded Na_2S active species into the pores of CMK-3 through a melting-casting method followed by a stress-release annealing-precipitation process, as shown in **Figure 8**a.[111] Owing to the reduced interface resistance and residential stress, the Na_2S-Na_3PS_4-CMK-3 nanocomposite delivered an extremely stable capacity of 810 mAh g^{-1} (based on the mass of Na_2S) at 50 mA g^{-1} at 60 °C, indicating the promising applications of this sulfur cathode in intermediate-temperature Na–S batteries. Moreover, Kaskel et al. reported a new approach to prepare Na_2S/hard carbon cathodes by employing the carbothermal reduction of Na_2SO_4 at different temperatures.[112] Such a structure enables high utilization of Na_2S components, leading to a stable capacity of 740 mAh g^{-1} for 36 cycles. Other Na_2S_x, such as Na_3S_4 and Na_2S_6, have also been employed to fabricate sulfur cathodes.[117–120] For example, Mitra et al. prepared a freestanding cathode using manganese dioxide-decorated carbon cloth (CC@MnO_2) as a polysulfide reservoir with Na_2S_6 solution as the active material.[119] Benefiting from the highly conductive electron pathways and efficient polysulfide adsorption capability, the as-obtained sulfur cathode showed an impressive specific capacity of 938 mAh g^{-1} with a remarkable capacity retention of ≈67% after 500 cycles (Figure 8b). These results suggest that long-chain sodium polysulfides are very promising for Na–S batteries.

3.1.3. Organosulfur Copolymer Cathodes

Designing organosulfur copolymer compounds to confine polysulfides via chemical bonding is another powerful strategy for preparing high-performance cathode materials for RT Na–S batteries. As a typical example, a polyacrylonitrile (PAN)/S covalent composite was fabricated by mixing the precursors, cyclization, and dihydrogen at 300 °C.[121–125] The strong covalent interaction between sulfur and the carbon backbone in PAN prevents the production of free long-chain polysulfides and leads to the uniform distribution of sulfur at the molecular level. As another advantage, PAN/S covalent composites are compatible with conventional carbonate electrolytes. These benefits make PAN/S composites very attractive for Na–S

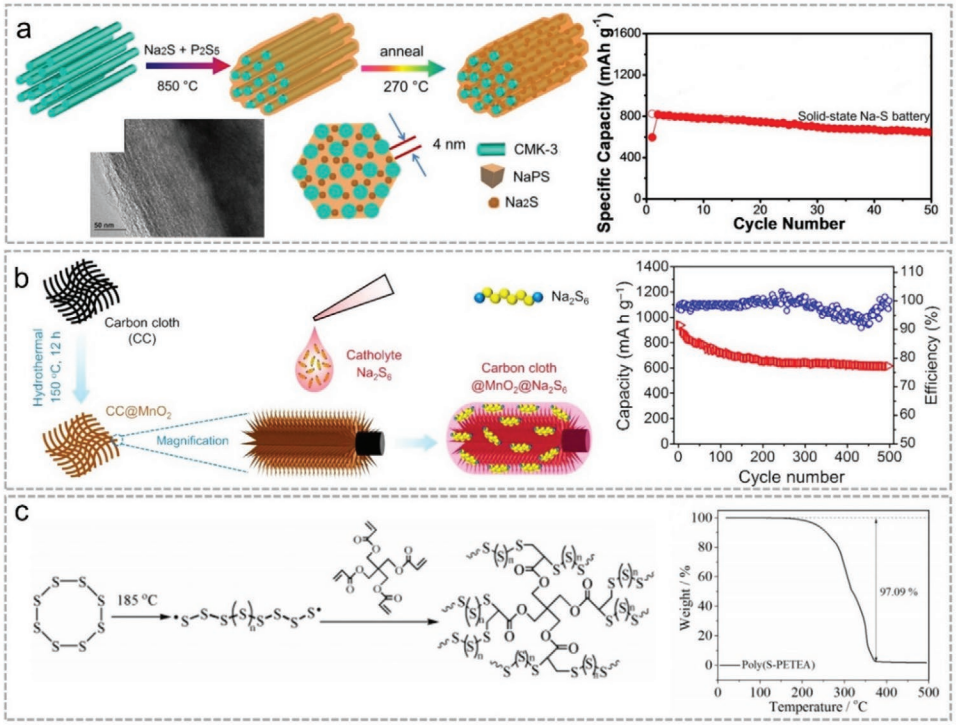

Figure 8. a) Schematic illustration of the synthesis of sodium sulfides in CMK-3 and their electrochemical performance in Na–S batteries. Reproduced with permission.[111] Copyright 2018, American Chemical Society. b) Synthesis and the electrochemical performance of CC@MnO_2@Na_2S_6 serving as the sulfur cathode in Na–S batteries. Reproduced with permission.[119] Copyright 2019, Elsevier. c) The chemical structure evolution of poly(S-PETEA) copolymer and the corresponding sulfur content measured by thermogravimetric analysis. Reproduced with permission.[32] Copyright 2018, Wiley-VCH.

batteries. For example, PAN/S covalent composites exhibited an initial capacity of 655 mAh g^{-1} based on the weight of the PAN/S composite.[126] Hwang et al. replaced PAN power with an electrospun PAN fiber mat to prepare a PAN/S composite cathode.[127] The 1D feature provided PAN/S nanofibers with better electrochemical performance, especially at high current densities. The fiber composite delivered a specific capacity of 153 mAh g^{-1} after 500 cycles at 1 C. Although PAN/S covalent composites exhibit ultra-stable cyclic performance, the low sulfur content in the composites (typically lower than ≈50 wt%) inevitably reduces the energy density.

To increase the sulfur content in the composite cathodes, Ghosh et al. reported a cardanol benzoxazine–sulfur composite (CS90) with a sulfur content of ≈90 wt%.[128] The as-prepared CS90 achieved a capacity of 542 mAh g^{-1} at 0.2 A g^{-1} and retained 335 mAh g^{-1} after 50 cycles. Another exciting result was reported by Zhou et al.,[32] who grafted sulfur onto a star-shaped crosslinking monomer, that is, pentaerythritol tetracrylate (PETEA). As shown in Figure 8c, S_8 was converted to diradical sulfur chains at 185 °C and was then copolymerized with the PETEA monomers to obtain S-rich poly(S-PETEA) covalent composites. The poly(S-PETEA) covalent composites had a sulfur content of as high as 97.1 wt%, and the composite sulfur cathode delivered a reversible capacity of 877 mAh g^{-1} at 0.1 C when a gel polymer electrolyte was used.[32]

In addition, small organosulfur molecules have also been employed to improve the electrochemical performance of RT Na–S batteries. A sulfur–carbon complex that relies on benzenedisulfonic acid and SO_4^{2-} was used as the sulfur source rather than elemental sulfur.[129] Because most sulfur exists in the form of O–S/C–S bridge-bonds (short/long-chain), the sulfur–carbon complex had sufficient interfacial contact and high ionic/electronic conductivities. Thus, the composites exhibited a specific capacity of 696 mAh g^{-1} at 2500 mA g^{-1} and excellent cyclic stability over 1000 cycles.

3.1.4. Metal Sulfide Cathodes

Metal sulfides with abundant sulfur atoms can form chemical bonds with polysulfides, providing a strong adsorption capability for soluble polysulfides during charge/discharge cycles. Thus, metal sulfides can serve as alternative sulfur cathodes for Na–S batteries. MoS_x,[130] Bi_2S_3,[131] FeS_2,[132] and Cu_2S[133] have thus far been developed as sulfur cathodes. Mullins et al. reported amorphous, sulfur-rich $MoS_{5.6}$ as the sulfur cathode for Na–S batteries (**Figure 9**a).[130] Owing to the stable sodium polysulfide retention, the $MoS_{5.6}$-based sulfur cathodes demonstrated a specific capacity of 537 mAh g^{-1} at 50 mA g^{-1} and a high rate capability of 200 mAh g^{-1} at 1.0 A g^{-1}. It should be noted that these values are calculated based on the mass of $MoS_{5.6}$, which is promising for practical applications. To further improve the electrical conductivity of metal sulfides, Chou et al. prepared a graphite-nanoplate-coated Bi_2S_3 composite for Na–S batteries (Figure 9b).[131] The as-prepared sulfur cathodes delivered an initial capacity of 550 mAh g^{-1} (based on the mass of Bi_2S_3@C), stable specific energy of 275–300 Wh kg^{-1} at 0.1 C, and superior cyclic stability with a negligible capacity decay of 0.3% per cycle.

In the above section, we systematically reviewed several types of sulfur cathodes for RT Na–S batteries. Multiple solutions have been proposed to optimize the physicochemical properties of nanocomposites to obtain a high sulfur content, high areal loading, and less polysulfide dissolution. The representative results are summarized in **Table 1**. However, notably, some important parameters such as the electrolyte/sulfur ratio, areal

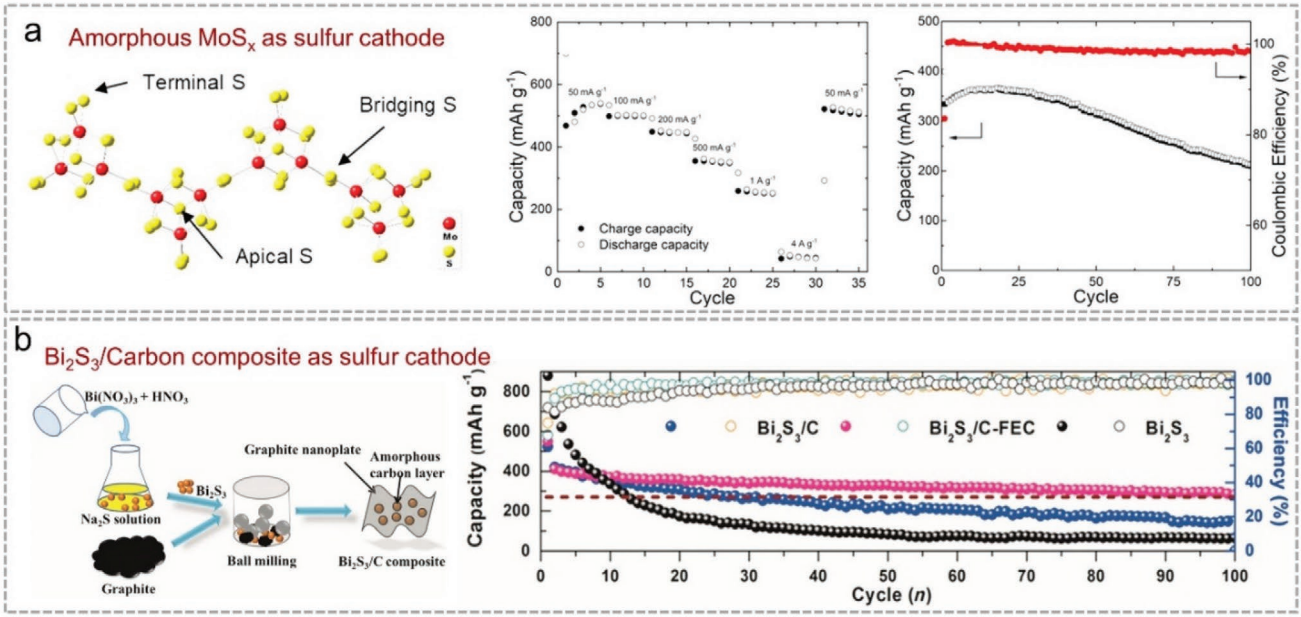

Figure 9. a) Structure and the electrochemical performance of amorphous MoS_x serving as the cathode of Na–S batteries. Reproduced with permission.[130] Copyright 2020, American Chemical Society. b) Synthesis of Bi_2S_3/C composite and its performance in Na–S. Reproduced with permission.[131] Copyright 2016, Wiley-VCH.

Table 1. Recent progress on the synthesis and electrochemical performance of sulfur cathodes for Na–S batteries.

Sulfur cathodes	Fabrication methods	Morphology	Sulfur content [wt %]	Sulfur loading [mg cm^{-2}]	Electrolyte	Rate performance[a]	Cyclic performance[a]	Ref.
N-doped graphene/sulfur	Chemical reaction deposition	Hierarchical porous structure	≈86	≈1.0	0.8 M $NaClO_4$ in ethylene carbonate(EC)/dimethyl carbonate (DMC) (v:v = 1:1)	212 mAh g^{-1} at 0.05 C	136 mAh g^{-1} after 10 cycles at 0.05 C	[59]
RGO/Mn_xO_y/sulfur	Chemical reactions	Layered porous structure	60.7	2.05	1 M $NaClO_4$ + 0.1 M $NaNO_3$ in tetraethylene glycol dimethyl ether (TEGDME)	425 mAh g^{-1} at 0.5 A g^{-1}	≈300 mAh g^{-1} after 400 cycles at 0.5 A g^{-1}	[60]
Carbon fiber cloth/sulfur	Thermal treatment	Porous structure	33.4	1–3	1.5 M $NaClO_4$ and 0.2 M $NaNO_3$ in TEGDME	390 mAh g^{-1} at 0.1 C	120 mAh g^{-1} after 300 cycles at 0.1 C	[63]
Carbon fiber/sulfur	Thermal treatment	Porous structure	57.19	0.79	Polyethylene oxide-based solid polymer electrolyte	713 mAh g^{-1} at 0.1 A g^{-1}	710 mAh g^{-1} after 100 cycles at 0.1 A g^{-1}	[64]
S_xSe_{1-x}/carbon fiber	Thermal treatment	Porous structure	49	0.8–1.0	1 M $NaClO_4$ in EC/propylene carbonate (PC) (w:w = 1:1)	1375 mAh $g^{-1}_{(Se_xS_{1-x})}$ at 0.1 A $g^{-1}_{(Se_xS_{1-x})}$	762 mAh $g^{-1}_{(Se_xS_{1-x})}$ after 100 cycles at 0.1 A $g^{-1}_{(Se_xS_{1-x})}$	[65]
$S_{0.6}Se_{0.4}$/carbon fiber	Electrospinning followed by annealing	Porous structure	57.45	0.9	1 M $NaClO_4$ in EC/PC (w:w = 1:1)	117 mAh $g^{-1}_{(Se_{0.6}S_{0.4})}$ at 1.0 A $g^{-1}_{(Se_{0.6}S_{0.4})}$	202 mAh $g^{-1}_{(Se_{0.6}S_{0.4})}$ after 160 cycles at 0.5 A $g^{-1}_{(Se_{0.6}S_{0.4})}$	[66]
Microporous carbon/sulfur	MOF precursor method	Porous polyhedron structure	65	0.73–1.0	1 M $NaClO_4$ in EC/PC (v:v = 1:1) with solid additive	600 mAh g^{-1} at 0.5 C	600 mAh g^{-1} after 100 cycles at 0.1 C	[67]
N-doped porous carbon/sulfur	MOF precursor method	Porous polyhedron structure	50	0.7–0.9	1 M $NaClO_4$ in TEGDME	≈1000 mAh g^{-1} at 0.1 C	500 mAh g^{-1} after 250 cycles at 0.2 C	[68]
S, N co-doped porous carbon skeleton/sulfur	MOF precursor method	Hierarchical porous structure	37	0.9–1.5	1 M $NaClO_4$ in PC+ 5 wt% fluoroethylene carbonate (FEC)	1262 mAh g^{-1} at 0.1 A g^{-1}	730 mAh g^{-1} after 1000 cycles at 1.0 A g^{-1}; 543 mAh g^{-1} after 1000 cycles at 5.0 A g^{-1}	[72]
N-doped mesoporous carbon nanosphere/sulfur	MOF precursor method	Hierarchical porous nanospheres	70.2	0.68–2.37	1 M M $NaClO_4$ in EC/PC (v:v = 1:1)	228 mAh g^{-1} at 2.0 C	639 mAh g^{-1} after 400 cycles at 0.1 C	[69]
Microporous carbon/sulfur	MOF precursor method	Porous structure	30	—	1 M $NaClO_4$ in EC/PC (v:v = 1:1) + 2 wt% FEC	—	556 mAh g^{-1} after 250 cycles at 0.1 C	[70]
Carbon microsphere/sulfur	MOF precursor method	Hollow porous structure	≈48	—	Sodium trifluoromethanesulfonate ($NaCF_3SO_3$) in diethylene glycol dimethyl ether (DEGDME)	617 mAh g^{-1} at 0.7 C	311 mAh g^{-1} after 60 cycles at 0.7 C	[71]
Carbon/sulfur	Commercially available	Porous structure	50	—	0.5 M $NaCF_3SO_3$ in TEGDME	≈1000 mAh g^{-1} at 0.1 C	—	[73]
Hard carbon/sulfur	Commercially available	Porous structure	—	—	1 M $NaCF_3SO_3$ in TEGDME	—	418 mAh g^{-1} after 160 cycles at 0.1 C	[74]
Carbon/sulfur	Template method	Interconnected porous structure	≈46	3.2–4.1	1 M $NaClO_4$ in EC/PC (v:v = 1:1) + 5 wt% FEC	127 mAh g^{-1} at 5.0 A g^{-1}	292 mAh g^{-1} after 200 cycles at 0.1 A g^{-1}	[75]
Ultra-microporous carbon/sulfur	Template method	Hierarchical porous structure	39.72	—	1 M $NaClO_4$ in EC/DEC (v:v = 1:1)	574 mAh g^{-1} at 1.0 C	392 mAh g^{-1} after 200 cycles at 1.0 C	[76]
N,S-doped carbon/sulfur	Template method	Hierarchical porous structure	22	1.1	1 M $NaClO_4$ in EC/PC (v:v = 1:1)	196 mAh g^{-1} at 2.3 A g^{-1}	400 mAh g^{-1} after 350 cycles at 0.23 A g^{-1}	[77]
Carbon sphere/sulfur	Template method	Hollow structure	60	—	$NaCF_3SO_3$ in TEGDME (molar ratio of 4:1)	550 mAh g^{-1} at 0.1 C	—	[78]

Table 1. Continued.

Sulfur cathodes	Fabrication methods	Morphology	Sulfur content [wt %]	Sulfur loading [mg cm^{-2}]	Electrolyte	Rate performance[a]	Cyclic performance[a]	Ref.
Carbon nanobeads-carbon nanosphere/sulfur	Template method	Hierarchical porous structure	44	—	1 M $NaClO_4$ in EC/PC (v:v = 1:1) + 5 wt% FEC	56 mAh g^{-1} at 2.0 A g^{-1}	290 mAh g^{-1} after 350 cycles at 0.1 A g^{-1}	[79]
Carbon sphere/sulfur	Biomass-derived method	Hierarchical porous structure	35	—	1 M $NaPF_6$ + 0.25 M $NaNO_3$ in TEGDME	700 mAh g^{-1} at 0.1 C	300 mAh g^{-1} after 1500 cycles at 1.0 C	[80]
Carbon carrier/sulfur	Biomass-derived method	Microporous structure	40	1.0	1 M $NaClO_4$ in EC/PC (v:v = 1:1) + 2 wt% FEC	1492 mAh g^{-1} at 0.1 C	95% capacity retention after 2000 cycles at 1.0 C	[81]
Carbon/sulfur	Carbonization of organic complex	Porous structure	38	1.2	1 M $NaClO_4$ in EC/DMC (v:v = 1:1)	500 mAh g^{-1} at 0.15 A g^{-1}	400 mAh g^{-1} after 150 cycles at 0.15 A g^{-1}	[82]
Carbon architecture/sulfur	Carbonization of organic complex	Porous structure	29	1.0–1.5	1 M $NaClO_4$ in EC/DMC (v:v = 6:4)	527 mAh g^{-1} at 2.0 A g^{-1}	1250 mAh g^{-1} after 500 cycles at 0.5 A g^{-1}	[83]
Carbon/sulfur	Carbonization of organic complex	Porous structure	21.5	0.9–1.1	1 M $NaClO_4$ in PC + 5 vol% FEC	≈300 mAh g^{-1} at 3.2 A g^{-1}	330 mAh g^{-1} after 800 cycles at 1.0 A g^{-1}	[84]
Carbon layer/sulfur	Wet-chemical synthesis	Layer porous structure	37.8	1.4–1.7	1 M $NaClO_4$ in EC/DEC (v:v = 1:1) + 5 wt% FEC	700 mAh g^{-1} at 8.1 C	811 mAh g^{-1} after 950 cycles at 1.6 C	[85]
CNTs/microporous carbon/sulfur	Template method	Hierarchical porous structure	40	—	1 M $NaClO_4$ in EC/PC (v:v = 1:1)	≈800 mAh g^{-1} at 2.0 C	—	[86]
CHNBs@PCNFs/sulfur	Electrospinning followed by thermal annealing	Hierarchical porous structure	71.2	1.4	1 M $NaClO_4$ in EC/PC (v:v = 1:1) + 5 wt% FEC	487 mAh g^{-1} at 2.0 C	256 mAh g^{-1} after 400 cycles at 2.0 C	[87]
Cu foam/sulfur	In situ growth method	Layered porous structure	—	—	1 M $NaClO_4$ in EC/PC (v:v = 1:1) + 5 wt% FEC	1403 mAh g^{-1} at 50 mA g^{-1}	—	[88]
Metal cluster/sulfur	Template method	Hollow structure	40	0.9–1.1	1 M $NaClO_4$ in EC/PC (v:v = 1:1) + 5 wt% FEC	220 mAh g^{-1} at 5.0 A g^{-1}	394 mAh g^{-1} after 1000 cycles at 0.1 A g^{-1}	[89]
Metal chalcogenide/sulfur	Hydrothermal method	Hollow structure	64.5	4.4	1 M $NaClO_4$ in TEGDME	349 mAh g^{-1} at 3.0 C	675 mAh g^{-1} after 800 cycles at 0.5 C	[90]
Atomic cobalt/carbon/sulfur	Thermal annealing	Porous hollow structure	48	5.0	1 M $NaClO_4$ in EC/PC (v:v = 1:1) + 5 wt% FEC	220.3 mAh g^{-1} at 5.0 A g^{-1}	508 mAh g^{-1} after 600 cycles at 0.1 A g^{-1}	[91]
Ni/N-doped CFs/sulfur	Electrospinning followed by annealing	Hierarchical porous structure	45	—	1 M $NaClO_4$ in TEGDME	181.7 mAh g^{-1} at 5.0 C	233 mAh g^{-1} after 270 cycles at 1.0 C	[92]
Carbon/Co/graphene aerogel/sulfur	Solution processing	Hierarchical porous structure	37.5	—	1 M $NaClO_4$ in EC/DEC (v:v = 1:1)	485 mAh g^{-1} at 0.5 C	226 mAh g^{-1} after 1000 cycles at 0.5 C	[93]
Co nanoparticles/CFs	Electrospinning followed by annealing	Nanoparticles embedded into CFs	38	≈1.0	1 M $NaClO_4$ in EC/DEC (v:v = 1:1)	906 mAh g^{-1} at 0.1 C	0.038% capacity decay for 800 cycles at 1.0 C	[94]
N-doped carbon sphere/Au/sulfur	Template method	Porous hollow structure	56.5	—	1 M $NaClO_4$ in PC + 5 wt% FEC	181 mAh g^{-1} at 20 A g^{-1}	369 mAh g^{-1} after 2000 cycles at 10 A g^{-1}	[95]
Carbon/sulfur/$BaTiO_3$/TiO_2	Electrospinning followed by ALD	Fabric-like structure	65	3.3–3.5	1 M $NaClO_4$ in EC/DEC (v:v = 1:1)	350 mAh g^{-1} at 2.0 A g^{-1}	382 mAh g^{-1} after 3000 cycles at 2.0 A g^{-1}	[96]
RGO/VO_2/sulfur	In situ grown method	Porous flower-like structure	40	—	1 M $NaClO_4$ in TEGDME	876 mAh g^{-1} at 0.2 C	156 mAh g^{-1} after 1000 cycles at 2.0 C	[97]

Table 1. Continued.

Sulfur cathodes	Fabrication methods	Morphology	Sulfur content [wt %]	Sulfur loading [mg cm^{-2}]	Electrolyte	Rate performance[a]	Cyclic performance[a]	Ref.
Carbon sphere@ MoS_2/sulfur	Template method followed by hydrothermal method	Porous hollow structure	44	—	1 M $NaClO_4$ in TEGDME	1309 mAh g^{-1} at 0.1 C	216.5 mAh g^{-1} after 1000 cycles at 1.0 C	[98]
NiS_2/N-CNTs/ sulfur	Solution processing	Hollow tube structure	32	2.5	1 M $NaClO_4$ in EC/PC (v:v = 1:1) + 3 wt% FEC	203 mAh g^{-1} at 5.0 A g^{-1}	401 mAh g^{-1} after 750 cycles at 1.0 A g^{-1}	[99]
Sulfur/ Na_3SbS_4/ carbon	Ball milling	Porous structure	—	6.34/12.74	Na_3SbS_4 solid electrolyte	662 mAh g^{-1} at 2.0 A g^{-1}	468 mAh g^{-1} after 100 cycles at 1.0 A g^{-1}	[100]
$CoNi_2S_4$/ sulfur/carbon	Solvothermal method	Layered structure	80	2.5–3.0	1 M NaTFSI in DOL/DME (v:v = 1:1)	180 mAh g^{-1} at 2.0 C	350 mAh g^{-1} after 100 cycles at 1/20 C	[101]
ZnS/CoS_2/ sulfur/carbon	Template method	Porous hollow structure	59	2.0	1 M $NaClO_4$ in EC/DEC (v:v = 1:1) + 5 wt% FEC	170 mAh g^{-1} at 5.0 A g^{-1}	250 mAh g^{-1} after 2000 cycles at 1.0 A g^{-1}	[102]
CoC_3/ Co-CNTs/ sulfur	Solution method followed by annealing	CNTs embedded into carbon cubes	≈77	3.2–8.6	1 M $NaClO_4$ in EC/DMC (v:v = 6:4)	1364 mAh g^{-1} at 0.1 C	79% capacity retention after 500 cycles at 2.0 C	[103]
VC/CNFs/ sulfur	Electrospinning followed by annealing	Porous fabric structure	42	—	1 M $NaPF_6$ in DOL/DME (v:v = 1:1)	295 mAh g^{-1} at 1.0 C	379 mAh g^{-1} after 2000 cycles at 0.5 C	[104]
CoP-Co/ carbon/sulfur	Carbonization followed by phosphidation	Porous hollow structure	53	1.7	1 M $NaClO_4$ in EC/PC (v:v = 1:1) + 3 wt% FEC	182 mAh g^{-1} at 5.0 A g^{-1}	448 mAh g^{-1} after 700 cycles at 1.0 A g^{-1}	[105]
Carbon black/ sulfur/AlOOH	Hydrothermal method	Porous layered structure	44.3	2.0	1 M $NaClO_4$ and 0.2 M $NaNO_3$ in TEGDME	392 mAh g^{-1} at 1.0 C	378 mAh g^{-1} after 500 cycles at 1.0 C	[106]
Na_2S-Na_3PS_4/ CMK-3	Melting-casting followed by annealing	Porous structure	—	—	Na_3PS_4 solid electrolyte	—	810 mAh $g^{-1}_{(Na_2S)}$ after 50 cycles at 0.05 A g^{-1} at 60 °C	[111]
Na_2S/hard carbon	Thermal reduction	Porous structure	—	—	1 M sodium bis(fluorosulfonyl)imide (NaFSI) in DEC/EC (v:v = 6:4) + 3 vol% FEC	350 mAh g^{-1} at 0.2 C	—	[112]
Na_2S/carbon matrix	Dissolution-precipitation	Hierarchical porous structure	—	—	1 M $NaPF_6$ in DEGDME/ DOL (v:v = 1:1) with 0.08 M of Na_2S and P_2S_5 as additives	690 mAh g^{-1} at 2.8 A g^{-1}	300 mAh g^{-1} after 200 cycles at 2.8 A g^{-1}	[113]
Na_2S/CNTs	Chemical reduction	Porous structure	—	—	1.5 M $NaClO_4$ + 0.3 M $NaNO_3$ in TEGDME	—	Stable for 100 cycles	[114]
Na_2S/ Activated CNFs	Self-weaving method	Porous structure	—	—	1.5 M $NaClO_4$ + 0.2 M $NaNO_3$ in TEGDME	—	Stable for 100 cycles at 0.2 C	[115]
Na_2S/ MWCNTs	Dripping-casting method	Porous structure	—	—	1.5 M $NaClO_4$ + 0.3 M $NaNO_3$ in TEGDME	—	380 mAh g^{-1} after 50 cycles at 1/3 C	[116]
Na_2S_6/ Activated carbon cloth (10.4 µL $mg_{(S)}$)	Alkaline treatment	Porous fiber surface	—	<2.0	0.5 M Na_2S_6 in (1.5 M $NaClO_4$ + 0.2 M $NaNO_3$)/ TEGDME	592 mAh g^{-1} at 2.0 C	678 mAh g^{-1} after 700 cycles at 0.5 C	[117]
Na_2S_6/CNFs/ Activated carbon	Dispersion-filtration	Porous structure	—	—	0.25 M Na_2S_6 in (1.5 M $NaClO_4$ + 0.2 M $NaNO_3$)/ TEGDME	800 mAh g^{-1} at 0.2 C	—	[118]
Na_2S_6/carbon cloth/MnO_2	Hydrothermal method	Porous layered structure	—	—	0.25 M Na_2S_6 in (1.5 M $NaClO_4$ + 0.2 M $NaNO_3$)/ TEGDME	938 mAh g^{-1} at 0.2 A g^{-1}	67% capacity retention after 500 cycles at 0.2 A g^{-1}	[119]

Table 1. Continued.

Sulfur cathodes	Fabrication methods	Morphology	Sulfur content [wt %]	Sulfur loading [mg cm^{-2}]	Electrolyte	Rate performance[a]	Cyclic performance[a]	Ref.
Na_3S_4/Ketjen black	As received	Porous structure	25	3.5	Na_3PS_4 solid electrolyte	340 mAh g^{-1} at 0.04 C	—	[120]
MXene nanosheets/ sulfur	Exfoliation method	Layered structure	58.75	2.1/4.5	2 M sodium trifluoromethane-sulfonimide (NaTFSI) in EC/PC (v:v = 1:1) + 5 wt% FEC	610 mAh g^{-1} at 5.0 C	577 mAh g^{-1} after 500 cycles at 2.0 C	[107]
2D MXene/ sulfur	Chemical synthesis	Layered structure	55	—	1.5 M $NaClO_4$ in TEGDME	120 mAh g^{-1} at 1.0 A g^{-1}	150 mAh g^{-1} after 300 cycles at 0.1 A g^{-1}	[108]
Te/sulfur/PAN	Chemical synthesis	Layered structure	42.06	1.0–1.2	1 M $NaClO_4$ in EC/DEC (v:v = 1:1) + 10% FEC and 1 M $NaClO_4$ in DME/DOL (v:v = 1:1) + 5 wt% FEC	629 mAh g^{-1} at 6.0 A g^{-1}	894 mAh g^{-1} after 500 cycles at 1.0 A g^{-1}	[122]
Sulfur/PAN	Sulfurized method	Layered structure	41	—	1 M $NaPF_6$ in EC/DEC (v:v = 1:1)	1473 mAh g^{-1} at 0.01 C	266 mAh g^{-1} after 200 cycles at 0.1 C	[123]
Se_xS_{1-x}@pPAN	Sulfurized method	Layered structure	44.6	1.0–2.0	1 M $NaClO_4$ in EC/PC (v:v = 1:1) and 1 M NaTFSI in TEGDME + 5 wt% FEC	767 mAh $g^{-1}_{(Se_xS_{1-x})}$ at 3.0 A $g^{-1}_{(Se_xS_{1-x})}$	770 mAh $g^{-1}_{(Se_xS_{1-x})}$ after 500 cycles at 0.4 A $g^{-1}_{(Se_xS_{1-x})}$	[124]
I-doped sulfur/ PAN	Sulfurized method	Layered structure	17.7	—	1 M $NaClO_4$ in EC/DEC (v:v = 1:1) + 8% FEC	994 mAh g^{-1} at 2.0 C	674 mAh g^{-1} after 500 cycles at 2.0 C	[125]
Sulfur/PETEA	Chemical bonding	—	3.36	—	Pentaerythritol tetraacrylate-based gel electrolyte	877 mAh g^{-1} at 0.1 C	736 mAh g^{-1} after 100 cycles at 0.1 C	[32]
2D MOFs/ sulfur	Solution processing	Layered structure	48.6	1 and 2.6	1 M $NaClO_4$ in EC/PC (v:v = 1:1) + 5 wt% FEC	284 mAh g^{-1} at 2.0 C	241 mAh g^{-1} after 1000 cycles at 2.0 C	[109]
Fe-PPy/sulfur	Solution processing	Porous structure	46	—	1 M $NaClO_4$ in EC/PC (v:v = 1:1) + 3 wt% FEC	205 mAh g^{-1} at 10 A g^{-1}	101 mAh g^{-1} after 1000 cycles at 0.3 A g^{-1}	[110]
Amorphous $MoS_{5.6}$	Solution-proceed method	Layered structure	40	1.5–2.0	1 M $NaPF_6$ in FEC/DEC (v:v = 1:1)	200 mAh $g^{-1}_{(MoS_{5.6})}$ at 1.0 A $g^{-1}_{(MoS_{5.6})}$	311 mAh $g^{-1}_{(MoS_{5.6})}$ at 1.0 A $g^{-1}_{(MoS_{5.6})}$ after 100 cycles	[130]
Bi_2S_3/graphite nanoplate	Precipitation method	Rod-like structure	—	—	1 M $NaClO_4$ in EC/DEC (v:v = 1:1)	550 mAh $g^{-1}_{(Bi_2S_3)}$ at 0.1 C	69% capacity retention after 100 cycles at 0.1 A g^{-1}	[131]
FeS_2 nanocrystals	Solution processing	Nanoparticles	—	—	1 M $NaPF_6$ in DEGDME	≈250 mAh $g^{-1}_{(FeS_2)}$ at 1.0 A $g^{-1}_{(FeS_2)}$	64% capacity retention after 30 cycles at 0.1 A g^{-1}	[132]
Cu_2S nanosheets	In situ reaction	Flake-like structure	—	>3.0	Varying concentration of Na_2S_6 in 1 M $NaSO_3CF_3$/ DEGDME	≈400 mAh g^{-1} at 1.0 A g^{-1}	Stable for 400 cycles	[133]

[a]Unless otherwise specified, the specific capacities in cyclic and rate tests are calculated based on the mass of sulfur.

loading of sulfur, and negative/positive capacity ratio, have been overlooked in early studies. These parameters are extremely important for practical applications, which is crucial for bridging the gap between industrial and fundamental research.

3.2. Electrolytes for Na–S Batteries

Electrolytes are another crucial component in batteries that affect the lifespan and reaction mechanisms of Na–S batteries. Different electrolytes have been explored for Na–S batteries, including organic liquids, gel polymers, and solid-state electrolytes.[134] Considering the similarity between the chemistries of Na–S and Li–S batteries, both ester and ether electrolytes were prepared by simply replacing the Li salts with their Na counterparts. Emerging Na salts including $NaClO_4$,[135] sodium trifluoromethanesulfonate ($NaCF_3SO_3$),[136–138] and NaTFSI[31] have thus far been adopted. Li et al. comprehensively studied the electrochemical properties of carbonate electrolytes for RT Na–S batteries. The highly concentrated electrolyte comprised NaTFSI salts, PC, and FEC.[31] It was demonstrated that the highly concentrated electrolyte not only prevented the dissolution of sodium polysulfides but also triggered a stable SEI layer on the Na surface. Impressively, by varying the salt

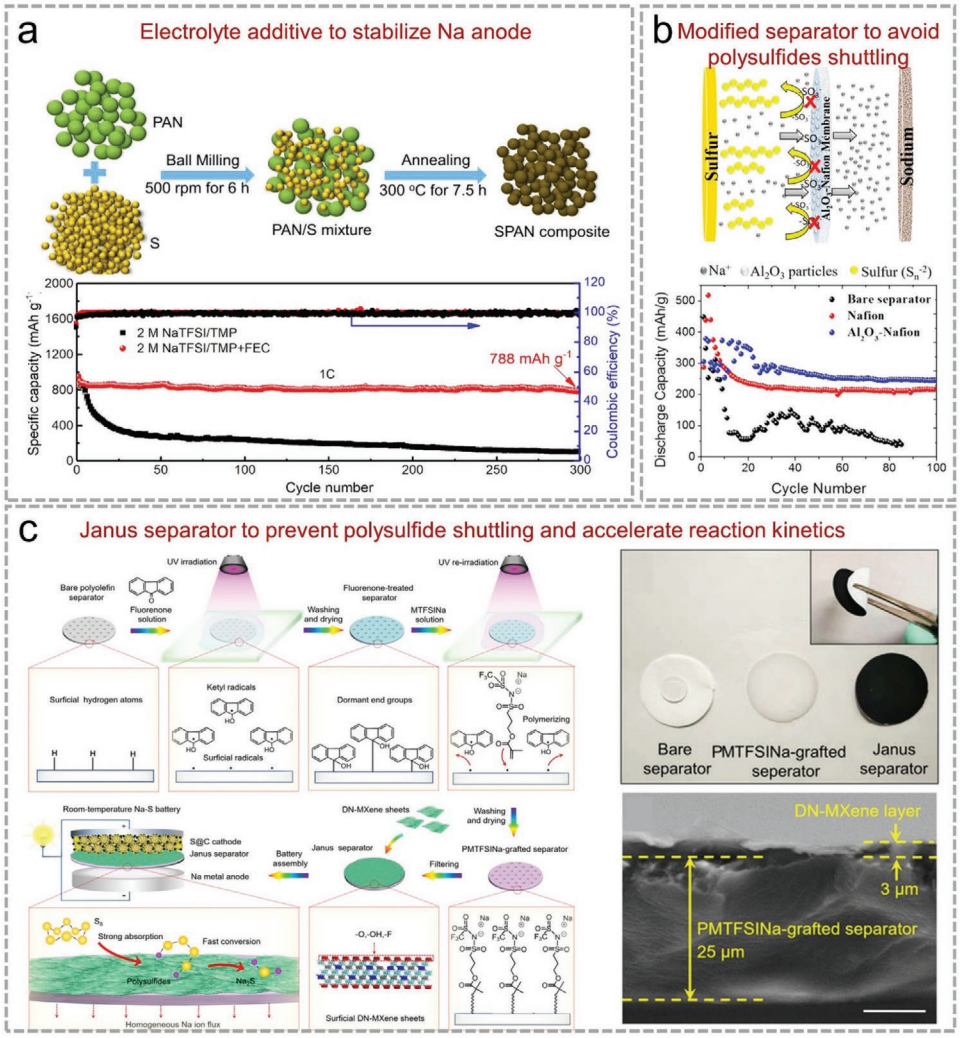

Figure 10. a) Synthesis of the SPAN composite and the electrochemical performance in 2 M NaTFSI/TMP and NaTFSI/TMP+FEC electrolytes. Reproduced with permission.[30] Copyright 2019, Elsevier. b) Schematic illustration of the Al_2O_3-Nafion interlayers and their electrochemical performance for Na–S batteries. Reproduced with permission.[145] Copyright 2019, American Chemical Society. c) Schematic illustration of the preparation of a Janus separator along with optical and cross-sectional SEM images. Reproduced with permission.[37] Copyright 2020, Wiley-VCH.

concentration, the electrochemical performance significantly fluctuates. Kim et al. reported a non-flammable electrolyte (2 M NaTFSI/trimethyl phosphate+FEC) for dendrite-free Na–S batteries (**Figure 10**a).[30] A high reversible capacity of 788 mAh g^{-1} after 300 cycles at 1.0 C was maintained with a capacity decay of only 0.04% per cycle. Theoretical simulations and surface analysis proved that the FEC additive was responsible for the excellent electrochemical performance.

Solid-state electrolytes are considered the ultimate choice for resolving the shuttle effect of polysulfides.[139–142] However, their low ionic conductivity and insufficient interfacial wetting with Na metal restrict their practical applications.[139] To overcome the abovementioned problems, Cheng et al. synthesized a solid electrolyte based on layered β-Al_2O_3 (BASE), which possesses extremely high RT ionic conductivity (≈1 mS cm^{-1}) and high chemical/mechanical stability.[140] The triple Na_xMoS_2-carbon-BASE nanojunction interface was constructed by adhering ternary Na anodes containing 3 wt% MoS_2 and 3 wt% carbon on BASE. The Na–S batteries using an all-solid-state electrolyte displayed a capacity of 1100 mAh g^{-1} at a current density of 1.5 mA cm^{-2}. All these findings demonstrate the great promise of all-solid-state electrolytes for practical applications.

3.3. Separator Modifications for Na–S Batteries

As mentioned above, both cathode construction and electrolyte optimization can improve the electrochemical performance of Na–S batteries by suppressing the dissolution and shuttle effect of sodium polysulfides. Separator modification is another feasible approach to achieve such goals, which has been widely used in Li–S batteries.[143,144] Because most sodium polysulfides are restricted at the cathode side, corrosion on the anode side is alleviated, resulting in much improved electrochemical performance, and in particular, long-term cyclic stability.[145–148] Demir-Cakan et al. reported an Al_2O_3/Nafion membrane to prevent the

migration of intermediate sodium polysulfides (Figure 10b).[145] Al_2O_3 is an effective adsorbent that chemically adsorbs sodium polysulfides, whereas the Nafion membrane allows the migration of Na^+ and repels sodium polysulfides. Consequently, the Na–S batteries exhibited a high capacity of 250 mAh g^{-1} after 100 cycles at 0.1 C. Moreover, an ion-selective polybenzimidazole (PBI) separator was adopted to suppress polysulfide shuttling.[146] It was revealed that the passivation of the final product, Na_2S_2, was the predominant attribute of large polarization and capacity fading. Thus, the RT Na–S batteries using such PBI separators exhibited excellent cyclability with a capacity retention of 92.9% for 50 cycles at 0.2 C, suggesting that separator modifications can be an efficient strategy to improve the electrochemical performance of Na–S batteries. Recently, Zhou et al. reported a Janus separator where one side was grafted with a single-ion-conducting polymer and the other side was coated with MXene (Figure 10c).[37] In such a separator, the grafting of the ion-conducting polymer not only improves the wettability of polyolefin separators in cyclic carbonate electrolytes but also renders dendrite-free Na deposition by uniforming the Na ion flux. In contrast, the MXene layer promoted the conversion reactions between polysulfides and Na_2S. When the Janus separator was employed, the RT Na–S batteries displayed a capacity of 962 mAh g^{-1} after 200 cycles at 0.1 C.

4. K–S Batteries

Compared with Li/Na–S batteries, research on K–S batteries has emerged because of the low redox potential and abundant reserves of K.[149] However, K is much more reactive than its Li and Na counterparts, and the larger ionic size of K^+ also results in sluggish reaction kinetics, hindering the practical applications of K–S batteries. To resolve these obstacles, both sulfur cathodes and electrolytes require rational design.

4.1. Sulfur Cathodes for K–S Batteries

Similar to Li–S and Na–S cathodes, various carbonaceous materials, such as CMK-3,[150] microporous carbon,[151] porous hard carbon,[152] and porous CNFs,[153] have been used to host sulfur for K–S batteries. Chen et al. reported a PANI-coated ordered mesoporous carbon (CMK-3)/sulfur composite, which showed an initial discharge capacity of 513 mAh g^{-1} and retained 202 mAh g^{-1} after 50 cycles at 50 mA g^{-1} (**Figure 11**a).[150] The capacities originated from the redox conversions between K_2S_3 and sulfur upon electrochemical cycles, as confirmed by transmission electron microscopy (TEM), XRD, and Raman

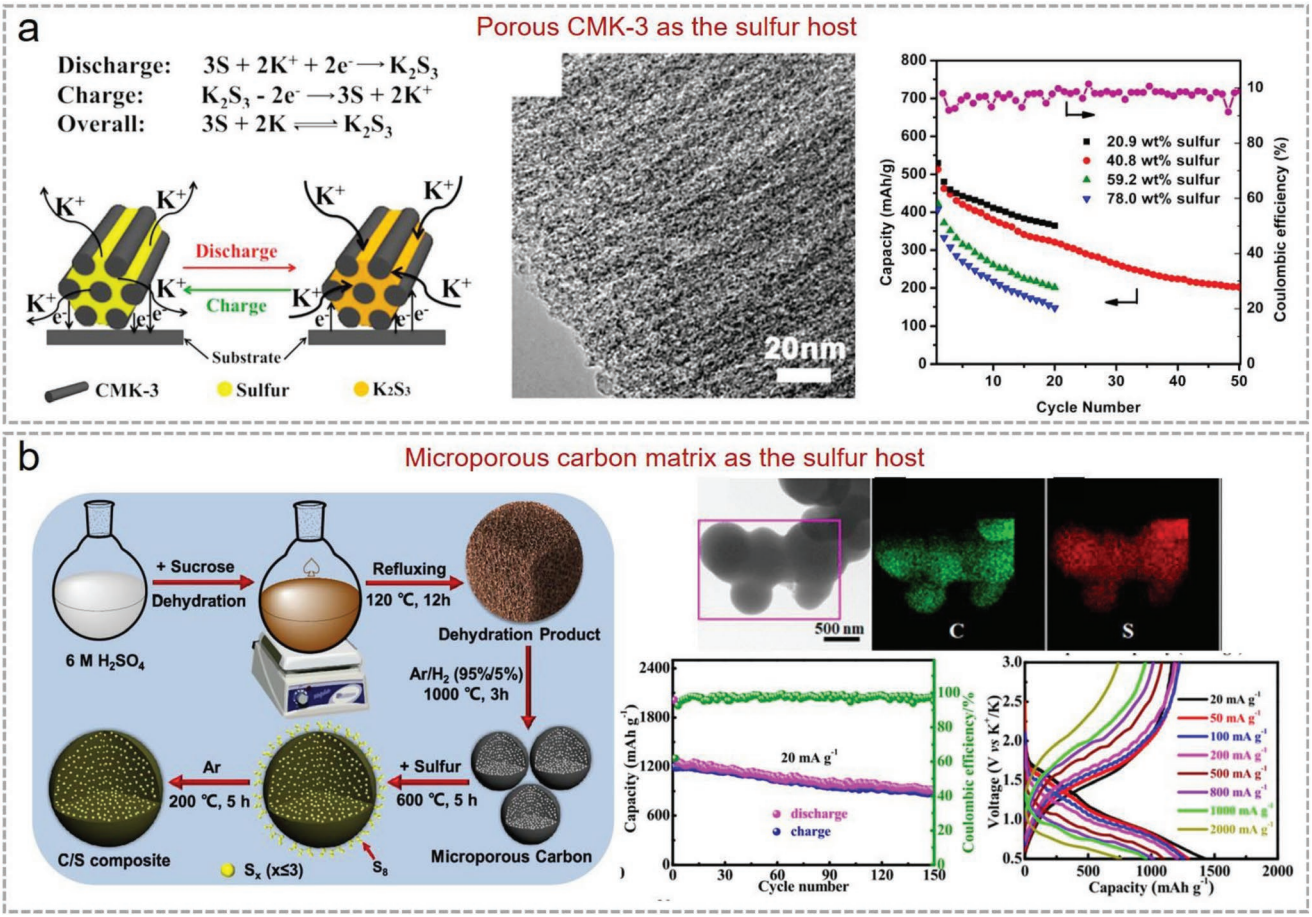

Figure 11. a) Schematic illustration, SEM image, and electrochemical performance of a CMK-3/S composite in K–S batteries. Reproduced with permission.[150] Copyright 2014, American Chemical Society. b) Synthesis, elemental maps, and electrochemical results of mesoporous carbon/S composite in K–S batteries. Reproduced with permission.[151] Copyright 2019, American Chemical Society.

Table 2. Recent progress on the synthesis and electrochemical performance of sulfur cathodes for K–S batteries.

Sulfur cathodes	Fabrication methods	Morphology	Sulfur content [wt%]	Sulfur loading [mg cm^{-2}]	Electrolyte	Rate performance	Cyclic performance	Ref.
CMK-3/S	Melt-diffusion	3D porous structure	40.8	—	1 M $KClO_4$ in TEGDME	512.7 mAh g^{-1} at 50 mA g^{-1}	202.3 mAh g^{-1} after 50 cycles at 50 mA g^{-1}	[150]
Microporous carbon/S	Melt-diffusion	3D porous structure	—	0.5–1.0 mg cm^{-2}	0.8 M KPF_6 in EC/DEC (v:v = 1:1)	1198.3 mAh g^{-1} at 20 mA g^{-1}	≈870 mAh g^{-1} after 150 cycles at 20 mA g^{-1}	[151]
Hard carbon/S	Melt-diffusion	Porous structure	—	—	0.5 M potassium bistrifluoromethanesulfonimide (KTFSI) in DEGDME	≈400 mAh g^{-1} at 0.1 C	—	[152]
CNFs/S	Electrospinning/Melt-diffusion	Porous structure	—	0.5–1.0 mg cm^{-2}	1 M potassium bis(fluorosulfonyl)imide (KFSI) in DME	1392 mAh g^{-1} at 20 mA g^{-1}	1002 mAh g^{-1} after 2000 cycles at 200 mA g^{-1}	[153]
PAN/S	Sulfurized process	Network structure	—	—	0.5 M KPF_6 in EC/DMC (v:v = 1:1)	550 mAh g^{-1} at 3.0 C	Capacity retention of 95% after 100 cycles at 0.5 C	[154]
PAN/S	Sulfurized process	Network structure	—	—	0.8 M KPF_6 in EC: DEC (v:v = 1:1)	710 mAh g^{-1} at 0.5 C	147 mAh g^{-1} after 100 cycles at 0.5 C	[155]
PAN/S	Sulfurized process	Particle structure	—	—	1 M KPF_6 in EC/DMC/ethyl methyl carbonate (EMC) (v:v:v = 4:3:2)	513 mAh g^{-1} at 35 mA g^{-1}	490 mAh g^{-1} after 100 cycles at 35 mA g^{-1}	[156]

spectra. In addition, Xu et al. confined small-molecule sulfur in microporous carbon for K–S batteries.[151] The strong confinement of small-molecule sulfur in the microporous carbon matrix eliminated the generation of soluble short-chain polysulfides and their shuttle effects. A reversible capacity of 1198 mAh g^{-1} was obtained with 72.5% capacity retention after 150 cycles (Figure 11b).

PAN/S can also be used as a sulfur cathode for K–S batteries.[154–156] Owing to their compositional and structural merits, K–S batteries using the PAN/S cathode displayed remarkable electrochemical performance. Wu et al. reported a pyrolyzed PAN/S nanocomposite as a cathode material for RT K–S batteries.[155] The PAN/S cathode delivered a high reversible capacity of 270 mAh g^{-1} and an outstanding rate capability of 83 mAh g^{-1} at 3.0 C. The detailed parameters of typical sulfur cathodes are provided in **Table 2**.

4.2. Electrolytes for K–S Batteries

The optimization of K–S battery electrolytes can efficiently suppress the dissolution and shuttle effect of polysulfides, thus enhancing battery performance. Potassium trifluoromethanesilfonimide (KTFSI) salt dissolved in 1,3-dioxolane/1,2-dimethoxyethane (DOL/DME) is a commonly used electrolyte; however, the shuttling of polysulfide in this ether electrolyte remains unsolved. To this end, Lu et al. developed a high-donor-number solvent, 1-methylimidazole (Me-Im), to reduce the solubility of polysulfides.[157] Me-Im promoted the reduction kinetics between K_2S_3 and K_2S, offering a high reversible specific capacity of 922 mAh g^{-1} and a gravimetric energy density of 1779 Wh kg^{-1}. Moreover, Sun et al. adjusted the concentration of KTFSI in tetraethylene glycol dimethyl ether (TEGDME) solvent to examine the effect of salt concentration on the electrochemical performance.[158] They showed that with a highly concentrated electrolyte (e.g., 5.0 M), the polysulfide shuttle effect was alleviated and the kinetics of polysulfide conversion was significantly enhanced. To synergistically restrict the polysulfide shuttle effect and protect the K metal anode, Lu et al. proposed a new K–S battery with a K^+-conducting BASE (K-BASE).[159] Novel K–S batteries displayed remarkable cyclic performance with almost no capacity decay for more than 1000 cycles, indicating great promise of high-performance K–S batteries.

5. Multivalent MSBs

5.1. Mg–S Batteries

Unlike Li/Na/K–S batteries with monovalent metals, multivalent metals are normally incompatible with typical organic liquid electrolytes. Moreover, enabling fast mass transportation of multivalent metal ions and reversible platting/stripping of multivalent metals in conventional electrolytes is still challenging. Although difficulties remain, Mg–S batteries are among the most cost-effective ones in terms of their high volumetric capacity (3832 mAh cm^{-3}), superior safety, high abundance, and low cost.[160–162]

5.1.1. Sulfur Cathodes for Mg–S Batteries

Analogous to alkali MSBs, sulfur/carbon composites are the most popular cathode design for Mg–S batteries (**Table 3**). A graphene-sulfur composite was prepared by thermal and chemical

Table 3. Recent progress on the synthesis and electrochemical performance of sulfur cathodes for multivalent MSBs.

Batteries	Sulfur cathodes	Fabrication methods	Morphology	Sulfur content (wt%)	Sulfur loading (mg cm^{-2})	Electrolyte	Rate performance	Cyclic performance	Ref.
Mg-S	RGO/S	In situ reduction	Porous layered structure	≈49	≈1.5	Magnesium–bis(hexamethyldisilazide) $[(HMDS)_2Mg]/AlCl_3/MgCl_2$ in TEGDME	108 mAh g^{-1} at 45 mA g^{-1}	219 mAh g^{-1} after 50 cycles at 20 mA g^{-1}	[163]
	Sulfide graphdiyne	Thermal pyrolysis	Porous layered structure	26.11	1.0	Anhydrous $AlCl_3$/LiCl in tetrahydrofuran (THF)	≈150 mAh g^{-1} at 250 mA g^{-1}	458.9 mAh g^{-1} after 36 cycles at 50 mA g^{-1}	[164]
	CNFs/S	Melt-diffusion	Network structure	—	≈1.0	$(HMDS)_2Mg/AlCl_3/MgCl_2$ in TEGDME	≈920 mAh g^{-1} at 0.1 C	—	[165]
	Ketjen black/S	Melt-diffusion	Porous structure	48	—	1.4 M $(HMDS)_2Mg/AlCl_3$ in TEGDME/DEGDME (v:v = 1:1)	768 mAh g^{-1} at 0.1 C	—	[166]
	Carbon/S	Melt-diffusion	Porous structure	41.3	0.6–0.7	0.4 M $(PhMgCl)_2/AlCl_3$ in THF	185.4 mAh g^{-1} at 0.2 C	210.4 mAh g^{-1} after 50 cycles at 0.1 C	[167]
	Co-carbon/S	MOF-derived method	Porous spherical structure	—	—	0.4 M $AlCl_3/MgCl_2$ in DME/PYR14TFSI (v:v = 1:1)	380 mAh g^{-1} at 0.4 C	High capacity for 400 cycles	[169]
	Co/N-carbon/S	MOF-derived method	Porous structure	47.1	≈1.0	$(HMDS)_2Mg/AlCl_3$ in DEGDME with LiTFSI additive	≈600 mAh g^{-1} at 1.0 C	450 mAh g^{-1} after 250 cycles at 0.1 C	[170]
	PAN/S	Thermal pyrolysis	Network structure	—	—	Magnesium tetrakis (hexafluoroisopropyloxy) borate $(Mg[B(hfip)_4]_2)$ in DME	422 mAh g^{-1} at 1/30 C	550 mAh g^{-1} after 20 cycles at 1/30 C	[172]
Al-S	Ketjen black/S	Melt-diffusion	Porous structure	—	1.1	$AlCl_3$ in 1-ethyl-3-methylimidazolium chloride ([EMIM]Cl)	≈1500 mAh g^{-1} at 30 mA g^{-1}	—	[196]
	Cu/carbon/S	MOF-derived	Porous structure	34	—	$AlCl_3$ in [EMIM]Cl (molar ratio of 1.3:1)	—	460 mAh g^{-1} after 500 cycles at 1.0 A g^{-1}	[197]
	CNTs/S	Melt-diffusion	Porous structure	—	—	$AlCl_3$ in [EMIM]Cl (molar ratio of 1.3:1)	1024 mAh g^{-1} at 100 mA g^{-1}	—	[198]
	Carbon cloth/S	Melt-diffusion	—	—	>1.0	$AlCl_3$ in [EMIM]Cl (molar ratio of 1.3:1)	≈1300 mAh g^{-1} at 50 mA g^{-1}	—	[199]
	PAN/S	Thermal annealing	Network structure	—	—	$AlCl_3$ in [EMIM]Cl (molar ratio of 1.5:1)	54 mAh $g_{(PAN/S)}^{-1}$ at 500 mA $g_{(PAN/S)}^{-1}$	201 mAh $g_{(PAN/S)}^{-1}$ after 20 cycles at 25 mA $g_{(PAN/S)}^{-1}$	[200]

precipitation methods, which were then used as the cathode for Mg–S batteries.[163,164] These architectures have several advantages: i) high electrical conductivity to ensure fast electron transfer; ii) strong chemical anchoring of sulfur species to alleviate the polysulfide shuttling; iii) mechanically stable frameworks to accommodate volume changes; iv) sufficient pores and voids to enable easy penetration of the electrolyte. Thus, Mg–S batteries exhibited a high specific capacity and remarkable long-term cyclic stability.[164] To further increase the sulfur content in carbonaceous materials, pores and voids require elaborate designs.[165–168] Wang et al. reported a cathode with a sulfur content of 64.7 wt% by embedding sulfur into a microporous carbon architecture.[167] As illustrated in **Figure 12**a, the sulfur host facilitated the physical confinement of polysulfide dissolution and shuttle effects. Consequently, the sulfur cathode exhibited an initial discharge capacity of 979 mAh g^{-1} at 0.1 C and retained 369 mAh g^{-1} after 200 cycles. The Co species were then incorporated into the carbon frameworks to accelerate the conversion of polysulfides during the charge/discharge processes.[169,170] Co species have strong chemical adsorption capability with polysulfides, and thus, prevent their dissolution and shuttle effect in the electrolyte. Wang et al. synthesized Co species embedded in a mesoporous carbon matrix (MesoCo@C) as a sulfur host. After melt impregnation of sulfur, the composites exhibited a high and stable capacity of 280 mAh g^{-1} for more than 400 cycles at 0.2 C (Figure 12b).[169] PAN/S covalent composites have also been explored for use in Mg–S batteries.[171–173] For instance, Wang et al. reported a PAN/S covalent composite with a sulfur loading of 47.3 wt%, which was prepared by directly heating the mixture of PAN

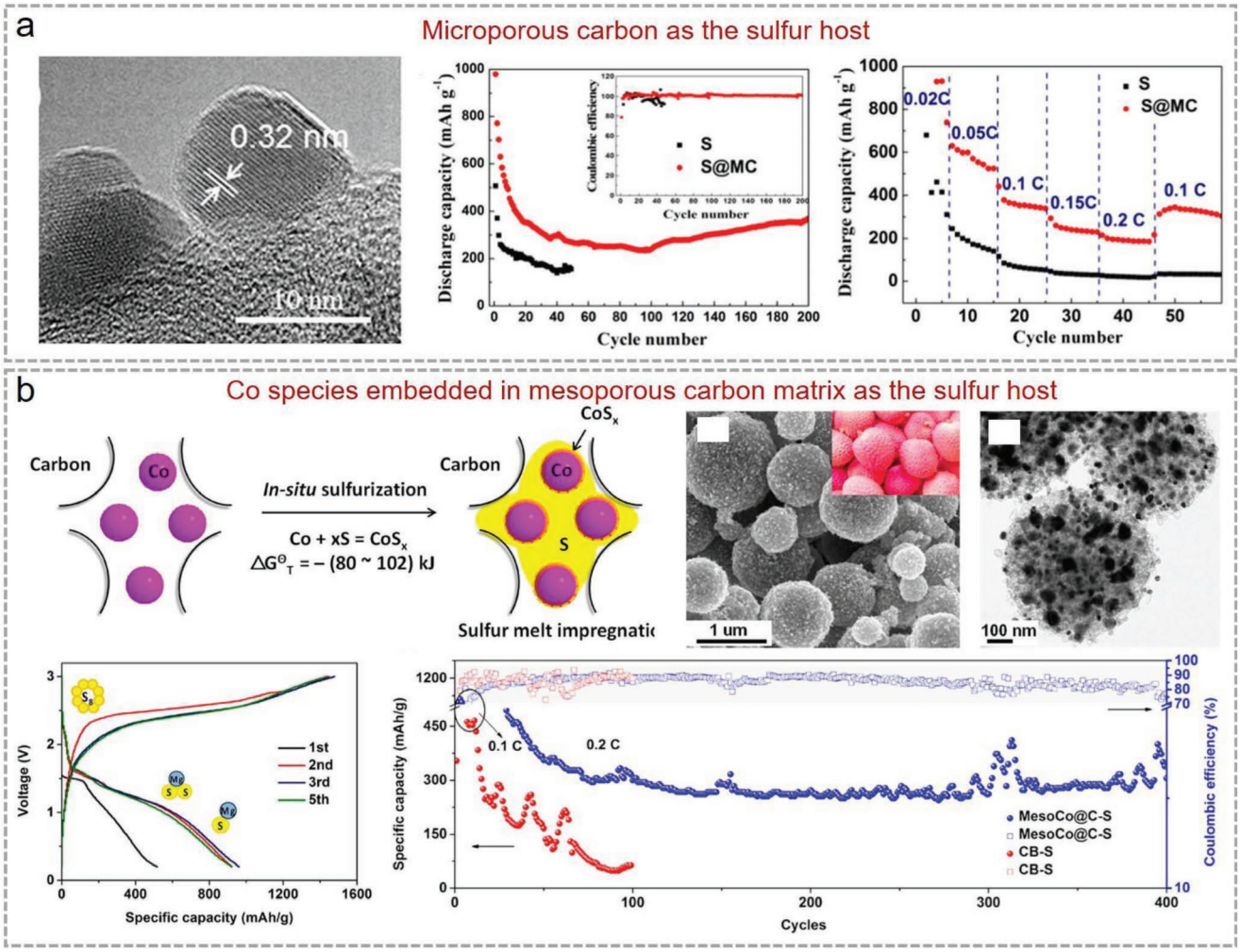

Figure 12. a) TEM image and electrochemical performance of a mesoporous carbon/sulfur composite as the cathode in Mg–S batteries. Reproduced with permission.[167] Copyright 2018, American Chemical Society. b) Schematic illustration of the synthesis, SEM and TEM images, and the electrochemical performance of carbon confined Co in mesoporous carbon serving as the sulfur host in Mg–S batteries. Reproduced with permission.[169] Copyright 2020, American Chemical Society.

powder and sulfur powder.[171] In general, S/PAN cathodes display better cyclic stability than carbon/sulfur composites.[172,173]

5.1.2. Electrolytes for Mg–S Batteries

Compared with the design of sulfur cathodes, it is much more challenging and crucial to design a suitable electrolyte for Mg–S batteries. Both Mg salts and solvents significantly affect the electrochemical performance of Mg–S batteries.[174,175] The first Mg salt used for the Mg–S battery electrolyte was $[Mg_2(\mu\text{-}Cl)_3(THF)_6]^{2+}$, which was reported by Muldoon et al. in 2011.[176] Since then, numerous Mg–S electrolyte systems have been explored. As a typical nucleophilic electrolyte, $(PhMgCl)_2$-$AlCl_3$/THF possesses good anodic stability and reversibility upon Mg deposition/dissolution cycles.[177] When employed for Mg–S batteries, a moderate capacity of 113 mAh g^{-1} was achieved after 20 cycles. In 2015, Fichtner et al. reported a new non-nucleophilic electrolyte composed of $(HMDS)_2Mg$ and diglyme/tetraglyme solutions for Mg–S batteries.[178] They achieved a discharge potential of ≈1.65 V for Mg–S batteries, close to the theoretical thermodynamic value, and a long upper voltage plateau with a relatively higher capacity was obtained. To date, various Mg compounds, such as $[(HMDS)_2Mg]$,[178–181] and MgCl-based,[182,183] have been developed as non-nucleophilic Mg electrolytes. Among them, the $(HMDS)_2Mg$ salt has several disadvantages, including corrosion problems of current collectors and inhibition of Mg transport. To resolve these pressing issues, Zhang et al. reported an electroactive salt, $[Mg(THF)_6][AlCl_4]_2$ (**Figure 13**a).[184] Because of their high Mg cyclic efficiency, good anodic stability, and high ionic conductivity, Mg–S batteries exhibited good cyclic performance for 20 cycles within the voltage range of 0.3–2.6 V, suggesting the reversible conversion of S to MgS without severe passivation of the Mg electrode surface.

To promote the practical applications of Mg–S batteries, several new electrolyte systems have been explored.[185–190] For instance, to broaden the voltage window of Mg compatible

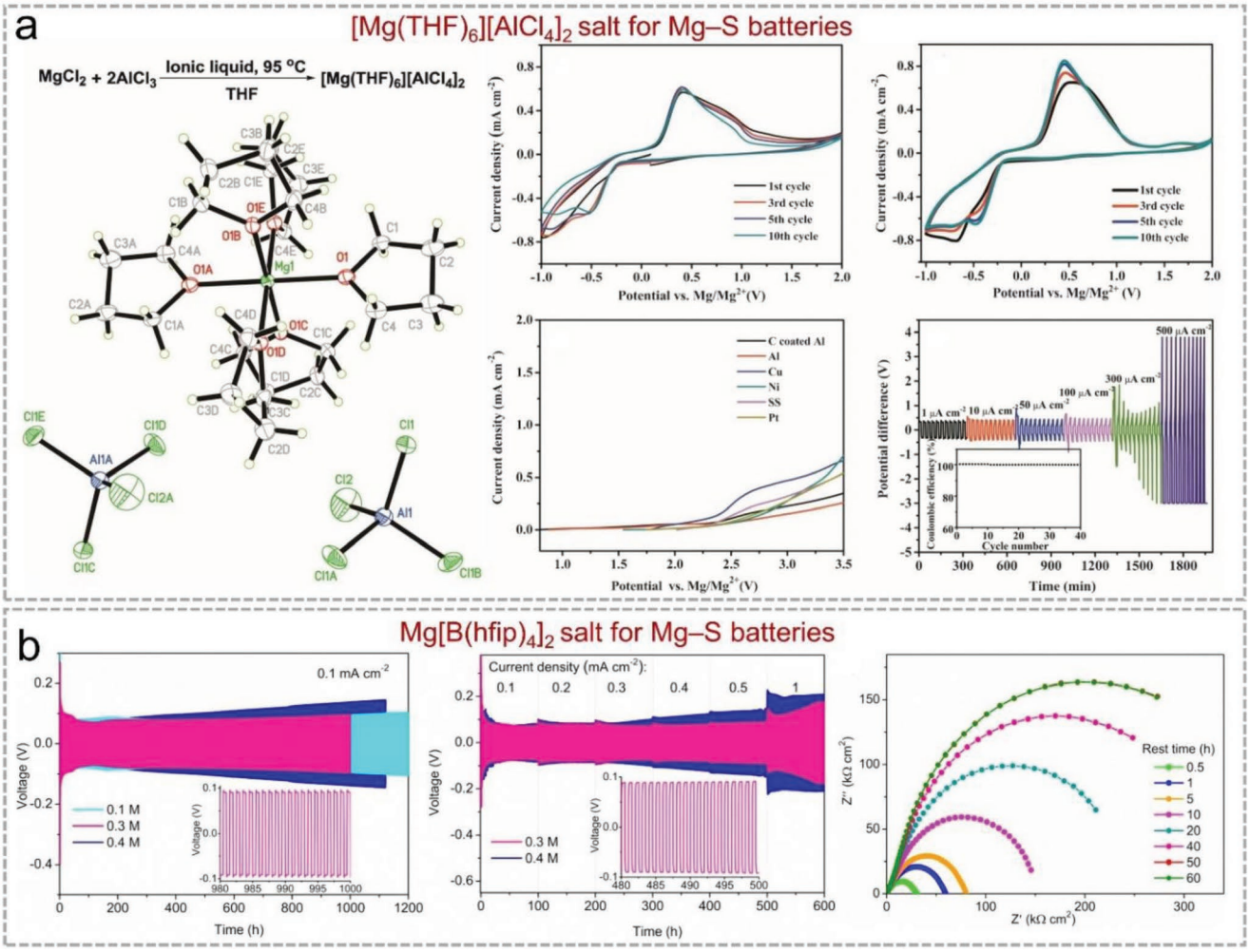

Figure 13. a) Molecular structure of $[Mg(THF)_6][AlCl_4]_2$ and electrochemical performance of Mg–S batteries obtained using $[Mg(THF)_6][AlCl_4]_2$ as the electroactive salt. Reproduced with permission.[184] Copyright 2016, Wiley-VCH. b) Electrochemical tests of Mg–S batteries by employing $Mg[B(hfip)_4]_2$ as the electrolyte. Reproduced with permission.[185] Copyright 2018, American Chemical Society.

electrolytes, Cui et al. reported a well-defined boron-centered anion-based Mg electrolyte (BCM electrolyte) by a facile one-step mixing strategy.[186] The electrolyte is characterized by easy synthesis, high ionic conductivity, compatibility with electrophilic sulfur, and non-corrosivity, thus resulting in an impressively prolonged cycle life. Moreover, Fichtner et al. reported an efficient and practical electrolyte comprising Mg tetrakic(hexafluoroisopropyloxy) borate ($Mg[B(hfip)_4]_2$).[185] Owing to its high anodic stability, high ionic conductivity, and excellent long-term Mg cyclic stability with low polarization (Figure 13b), the electrolyte exhibited excellent electrochemical performance. Meanwhile, Wang et al. developed a new electrolyte by dissolving $Mg(CF_3SO_3)_2$-$AlCl_3$ in tetrahydrofuran and a tetraglyme co-solvent.[187] The electrolyte exhibited a low overpotential, moderate anodic stability, suitable ionic conductivity, and good compatibility with the sulfur cathode. Although significant improvements have been achieved, the feasibility of Mg–S batteries remains a subject of debate. More efforts are urgently needed to commercialize Mg–S batteries.

5.2. Ca–S Batteries

Ca is another earth-abundant element, making Ca–S batteries a promising high-energy-density system. See and Seshadri first reported the Ca–S chemistry in 2013;[191] however, the as-formed system was not reversible because of the difficulty in Ca plating.[192] Subsequently, numerous studies have focused on the exploration of new electrolyte systems and the introduction of electrolyte additives to improve the electrochemical performance of Ca–S batteries.[193–195] For instance, Zhao-Karger et al. developed a new electrolyte system composed of Ca tetrakis (hexafluoroisopropyloxy) borate ($Ca[B(hfip)_4]_2$) for Ca–S batteries.[193] The obtained Ca–S batteries show a high cell voltage of 2.1 V; however, the cyclic stability was not satisfactory. With a sulfur/activated carbon cloth as the sulfur cathode, Stievano et al. examined the electrochemical activity of Ca–S batteries using an alkoxyborate-based electrolyte.[194] In situ and ex situ characterizations verified that elemental sulfur could be successfully retained at the end of each charge process, indicating reversible charge/discharge processes. In addition, Manthiram et al.

demonstrated that a Li^+-mediated Ca-based electrolyte could further improve the reversibility of the Ca–S chemistry and utilization of sulfur cathodes.[195] These investigations pave the way for exploring alternative multivalent MSBs.

5.3. Al–S Batteries

Al is the most abundant metal element (≈8.1%) on the Earth's crust. Regarding the remarkable specific gravimetric capacity of 2980 mAh g^{-1} and volumetric capacity of 8050 mAh cm^{-3}, Al is very promising for battery applications, such as Al-ion batteries and Al–S batteries.

5.3.1. Sulfur Cathodes for Al–S Batteries

Published research on sulfur cathodes for Al–S batteries has mostly focused on the construction of sulfur/carbon composites (Table 3). For example, composites using Ketjen black as the host were prepared as cathode materials. When an ionic liquid (IL) electrolyte was employed, the assembled Al–S batteries delivered an impressive discharge capacity of 1400 mAh g^{-1} (based on sulfur), accompanied by a discharge plateau of ≈1.2 V.[196] In another work, Ji et al. prepared a sulfur cathode by anchoring sulfur on a MOF-derived carbon matrix.[197] XRD and Auger spectrum results revealed that the Cu in MOF (HKUST-1) formed S–Cu ionic clusters, thus facilitating the electrochemical reaction and improving the reversibility of S upon charging/discharging. Meanwhile, Cu increased the electron conductivity at the carbon matrix/S interface, which significantly reduced the kinetic barrier for the conversion of sulfur species during battery operation. Thus, the S@MOF-derived carbon composite exhibited a reversible capacity of 600 mAh g^{-1} at the 75th cycle and a reversible capacity of 460 mAh g^{-1} after 500 cycles at 1 A g^{-1} (**Figure 14**a). In addition, activated carbon cloth and self-woven CNF paper were reported as sulfur hosts, and S/PAN was examined as a sulfur cathode.[198–201]

5.3.2. Electrolytes for Al–S Batteries

Typically, the plating/stripping of Al is reversible in IL electrolytes. Therefore, various IL-based electrolytes have been

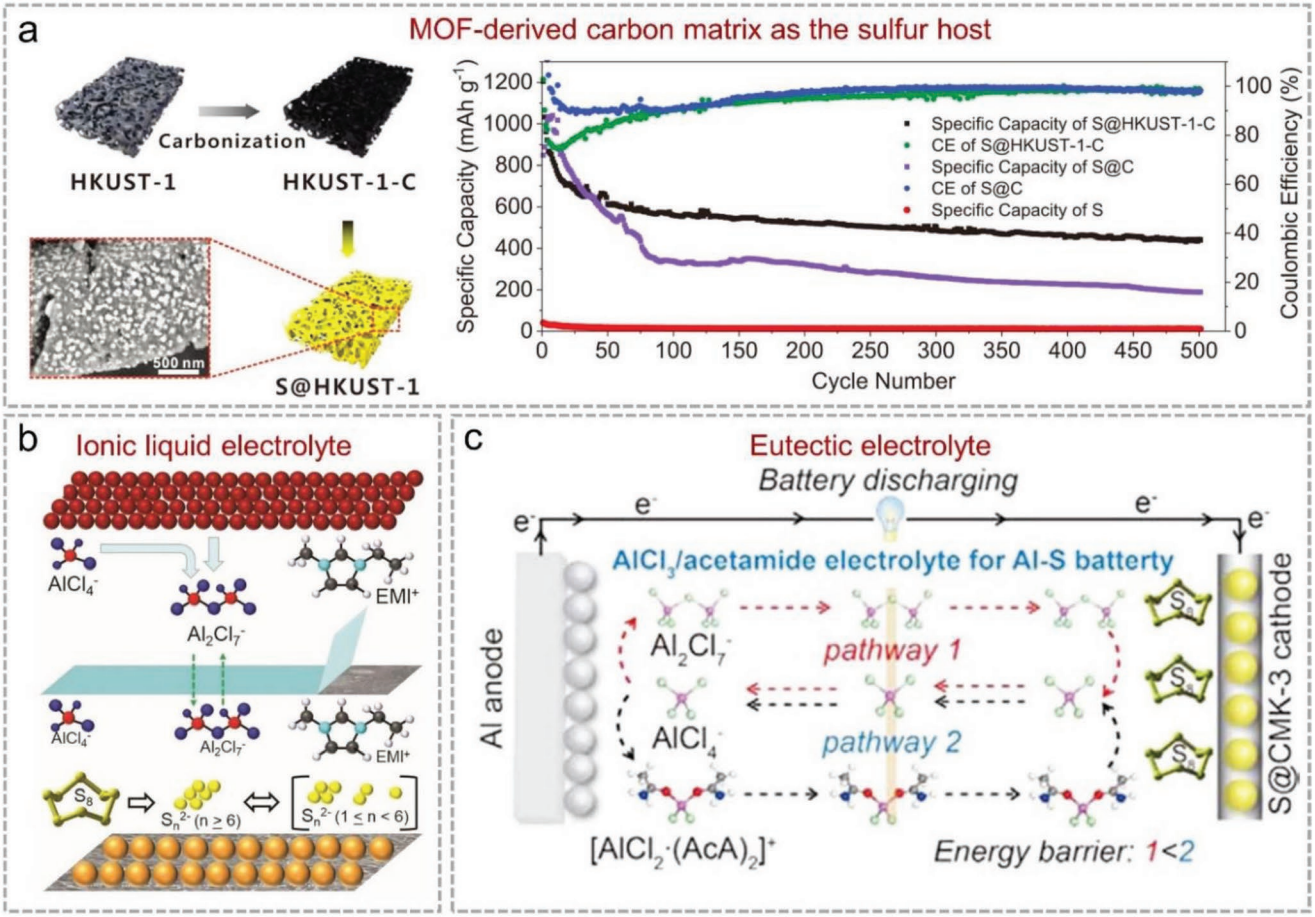

Figure 14. a) Synthesis of S@HKUST-1 composite and the electrochemical performance of S@HKUST-1 cathode for Al–S batteries. Reproduced with permission.[197] Copyright 2019, Wiley-VCH. b) Schematic diagram of the charge/discharge mechanism of Al–S batteries using the EMIMBr-$AlCl_3$ electrolyte. Reproduced with permission.[202] Copyright 2017, Wiley-VCH. c) Schematic illustration of the discharge process of Al–S batteries with an $AlCl_3$/acetamide eutectic electrolyte. Reproduced with permission.[209] Copyright 2019, Elsevier.

developed over the last decade. A commonly used electrolyte solution is the IL, 1-ethyl-3-methylimidazolium chloride (EMIMCI)-$AlCl_3$, which is prepared by mixing $AlCl_3$ in the organic cation chloride salt EMIMCI with different molar ratios.[196,198,199,202–204] Wang et al. reported a rechargeable Al–S battery using the EMIMCI-$AlCl_3$ electrolyte with a molar ratio of 1.3:1.[199] The sulfur in the cathode undergoes a solid-state conversion reaction with large voltage hysteresis, which is caused by slow reaction kinetics. Moreover, using the same electrolyte, Yu et al. demonstrated that high-order polysulfides (S_x^{2-}, $x \geq 6$) are soluble in the IL electrolyte, and transitions between S_6^{2-} and insoluble low-order polysulfides are reversible, as illustrated in Figure 14b.[202] By replacing EMIMCI with 1-ethyl-3-methylimidazolium bromide (EMIMBr), Li et al. reported a new IL electrolyte, called EMIMBr-$AlCl_3$.[205] $Al_2Cl_6Br^-$ served as the dissociation reaction reagent, instead of $Al_2Cl_7^-$, in a kinetically accelerated Al–S battery, which has a sulfur utilization higher than 80%. In addition, Manthiram et al. reported a Li^+-ion mediation strategy to enhance the reversibility of RT Al–S batteries. The electrolyte was prepared by mixing $AlCl_3$ and solid EMIMCl, followed by dissolving additional Li salt ($LiCF_3SO_3$) into the above IL.[206] Experimental and theoretical results suggested that the enhancement in reversibility can be attributed to the presence of Li^+, which promotes the formation of soluble polysulfides and therefore reduces the kinetic barrier for the reduction and oxidation of Al polysulfides. Thus, the Al–S batteries exhibited an initial capacity of 1000 mAh g^{-1} and maintained a high specific capacity of 600 mAh g^{-1} after 50 cycles. To further enhance the chemical stability of sulfur in IL electrolytes, Bian et al. developed a new $AlCl_3$/urea electrolyte for Al–S batteries.[207] Operating with this electrolyte, the Al–S batteries displayed a high specific capacity of ≈700 mAh g^{-1} and retained 500 mAh g^{-1} after 100 cycles.

Apart from IL-based electrolytes, several new electrolyte systems have also been developed for Al–S batteries.[208,209] For instance, Ji et al. fabricated a water-in-salt electrolyte composed of a mixture of aluminum trifluoromethanesulfonate ($Al(OTF)_3$), lithium bis(trifluoromethanesulfonyl)imide (LiTFSI), and hydrochloric acid (HCl) in deionized water.[208] The presence of LITFSI trapped the water molecules and inhibited the hydrolysis of polysulfides in the electrolyte, whereas the mildly acidic environment enabled repeatable oxidation/reduction reactions at the anode. Moreover, $AlCl_3$ was dissolved in acetamide under stirring and was employed as the electrolyte in RT Al–S batteries (Figure 14c).[209] XRD characterization demonstrated the generation of aluminum sulfides, including Al_2S_3, as the electrochemical conversion products. The Al–S batteries delivered a specific capacity of 1500 mAh g^{-1} and a high rate capability (688 mAh g^{-1} at 300 mA g^{-1}).

6. Advanced Characterization Techniques

To gain an in-depth understanding of the electrochemical reactions of non-lithium MSBs, advanced characterization techniques, including in/ex situ XRD, Raman, X-ray photoelectron spectroscopy (XPS), TEM, and energy X-ray absorption fine structure (EXAFS), have been employed to provide useful information regarding charge and discharge products.

In situ characterizations monitor real-time electrochemical reactions, which help probe the generation of intermediates and further conversion of metal polysulfides.[75,79,81,90–93,95,98,99,101,102,153] In situ synchrotron XRD is a powerful technique to probe the crystallographic intermediates, which has been widely employed in the mechanistic studies of MSBs.[75,79,90,91,95,99,102] For instance, Dou et al. conducted in situ XRD to track the conversions of intermediate polysulfides under different working stages, as shown in **Figure 15**a.[91] They showed that cobalt catalyzed Na_2S_4 into elemental sulfur during the charge process, whereas irreversible Na_2S_4 species were detected without the cobalt catalyst. With cobalt as the catalyst, elemental sulfur can be fully converted into Na_2S, resulting in better sulfur utilization. To further explore the chemical conversion reactions, Chou and co-workers monitored the phase evolution of a core-shell structured multisulfiphilic cathode using an in situ synchrotron XRD technique.[102] The XRD patterns revealed that the S_8 molecules could be fully transformed into long-chain polysulfides, followed by Na_2S. Similarly, the in situ XRD technique confirmed the catalytic functions of cobalt atoms[91] and metal sulfides.[90,99]

In situ Raman spectroscopy is another widely employed tool for determining the detailed working mechanisms of non-lithium MSBs.[92,93,98,101] With the hollow carbon sphere@MoS_2 as the sulfur host, Xu et al. employed in situ Raman spectroscopy to investigate polysulfide conversions.[98] Because MoS_2 and sodium polysulfides have different Raman peaks, the appearance and disappearance of Raman peaks at different charge/discharge statuses reflect the evolution of intermediates, thus highlighting the actual working mechanisms. As shown in Figure 15b, elemental sulfur underwent a two-step conversion reaction process, converting into long-chain polysulfides (Na_2S_x, $4 \leq x \leq 8$), followed by short-chain polysulfides (Na_2S_2/Na_2S). Moreover, Xu et al. probed intermediate polysulfide conversions in Na–S batteries, when Ni hollow sphere@N-doped carbon fibers were used as the sulfur host.[92] In situ Raman spectroscopy demonstrated that the peaks of S_8 molecules existed during the entire discharge process. This observation indicated that S_8 was not completely reduced, which could be attributed to the sluggish reaction kinetics of the Na–S batteries. During the charging process, the polysulfides were partially oxidized to sulfur because of the presence of both elemental sulfur and Na_2S.

In situ TEM[153] and in situ ultraviolet-visible (UV–vis) spectroscopy[81] were also used to reveal the working mechanisms. Xu et al. performed in situ TEM to examine the stability of porous carbon nanofiber (PCNF)/S cathode during the potassiation/depotassiation processes.[153] As shown in Figure 15c, the diameter of the PCNF/S composite fiber increased from 180 to 240 nm, with an increment of 33% during the discharge process. Impressively, the PCNF host maintained its initial morphology and structure after the full depotassiation process, indicating the excellent structural stability of the PCNF/S composite. In contrast to the above discussions, Xia et al. conducted in situ UV–vis spectroscopy to probe the working mechanisms of an ultra-porous carbon host in Na–S batteries.[81] Notably, Na_2S was the only product during the whole discharge process. During the charge process, the peaks corresponding to elemental sulfur were measured, indicating one-step conversion mechanisms in Na–S batteries.

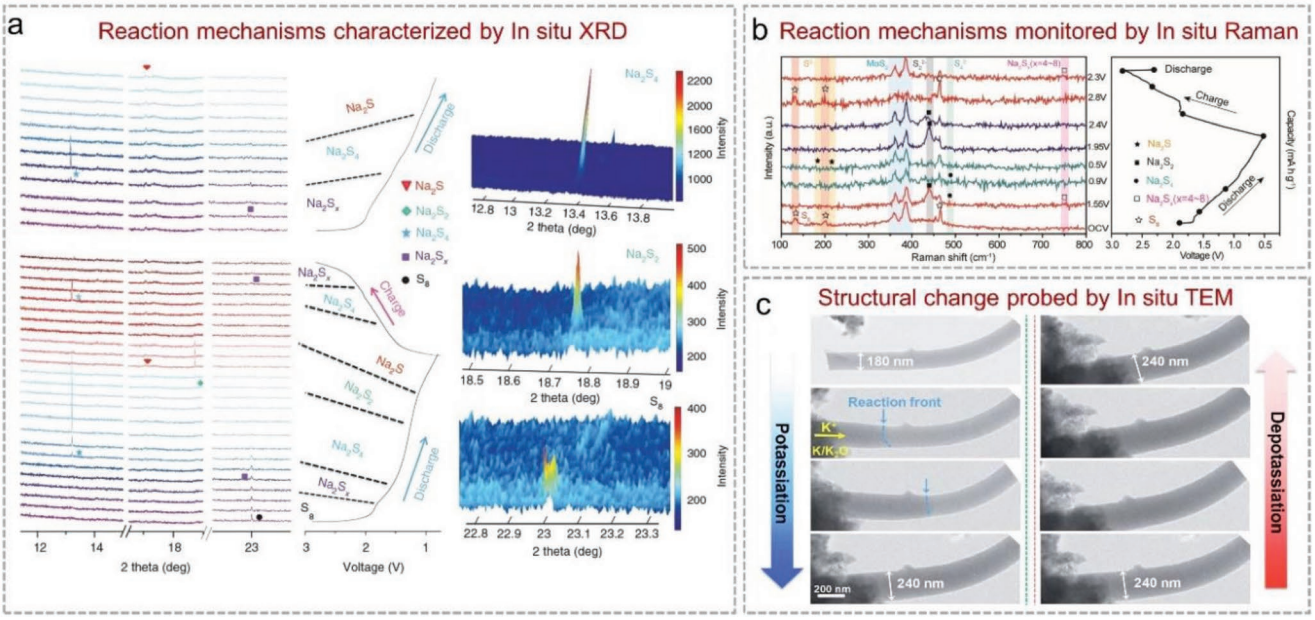

Figure 15. a) In situ synchrotron XRD patterns of the Na–S batteries comprising an atomic cobalt-decorated hollow carbon host with the initial galvanostatic charge/discharge curves at 500 mA g^{-1}. Reproduced with permission.[91] Copyright 2018, Nature Publish Group. b) In situ Raman analysis of the S@HCS/MoS_2 electrode at different discharge stages. Reproduced with permission.[98] Copyright 2019, Wiley-VCH. c) In situ TEM images of the PCNF/S cathode during potassiation/depotassiation processes. Reproduced with permission.[153] Copyright 2020, Royal Society of Chemistry.

Ex situ characterizations, such as ex situ XRD, ex situ Raman, and ex situ XPS, also provide useful information for understanding the reaction mechanisms of non-lithium MSBs. The ex situ XRD technique is an easily manipulated tool to probe the generation of metal polysulfides during charge/discharge cycles because different polysulfide intermediates show distinct XRD peaks.[94,131,158] For instance, Chou et al. applied ex situ XRD to study the storage behavior of Bi_2S_3, which was directly used as the cathode material for Na–S batteries.[131] As shown in **Figure 16**a, diffraction peaks attributed to Na_2S appeared when the cell was discharged to 0 V, whereas the diffraction peaks of elemental sulfur were observed after the first charge process, suggesting the conversion between Na_2S and elemental sulfur during the first cycle. Wang et al. performed ex situ XRD to study the redox reactions in K–S chemistry.[158] The XRD results confirmed that the K–S batteries underwent a multistep conversion between S_8 molecules and K_2S_3 during charge/discharge processes, indicating that the K_2S_3 phase is an electrochemically stable product in the concentrated electrolyte, that is, 5 M KTFSI in diglyme.

Ex situ Raman spectroscopy has also been employed to probe phase transformation in non-lithium MSBs.[31,72,83,84,154,155] Ex situ Raman spectra of Na–S batteries were collected during the first two discharge and charge processes, as shown in Figure 16b.[72] The presence of the C-S peak and the disappearance of the S-S peak implied the conversion of S_8 molecules into Na_2S, which was confirmed by other studies that used covalent polymer-sulfur cathodes.[83,154,155] Moreover, Kang et al. conducted ex situ Raman spectroscopy to track the evolution of sulfur species during charge/discharge processes, and their results demonstrated that solid Na_2S was formed during the initial discharge process, which could not be fully oxidized during the following charge cycle because of the poor kinetics for transferring the short-chain polysulfides.[31] It has also been reported that Na_2S_x ($4 \le x \le 8$) can be generated from Na_2S in the presence of I_3^-, because the peak intensity of Na_2S_x remains strong even after charge/discharge cycles.

Apart from the above-mentioned in/ex situ characterizations, new characterization techniques, such as EXAFS, were also conducted in non-lithium MSBs.[105] According to the EXAFS results, Chou et al. proposed that the released electronegativity of phosphorus and the electron delocalization of Co in the CoP-Co composite was responsible for the high electrocatalytic activity of sodium polysulfide conversions (Figure 16c).[105] Moreover, porous hollow structures and highly active heterostructures promote polysulfide adsorption and electron transfer, whereas CNTs offer a highly conductive network and provide synergistic effects of physical confinement and chemical anchoring of polysulfides.

7. Conclusions and Perspectives

Non-lithium MSBs have attracted considerable interest because of their high energy densities, high specific capacities, and low costs. Unfortunately, the severe shuttle effect of polysulfides, the low electronic conductivity of sulfur and polysulfides, the large volume expansion of elemental sulfur, and the sluggish reaction kinetics have restricted their commercial applications. Numerous efforts have been devoted to circumventing these challenges, including the modulation of nanostructured cathodes, optimization of electrolyte formulas, and utilization of

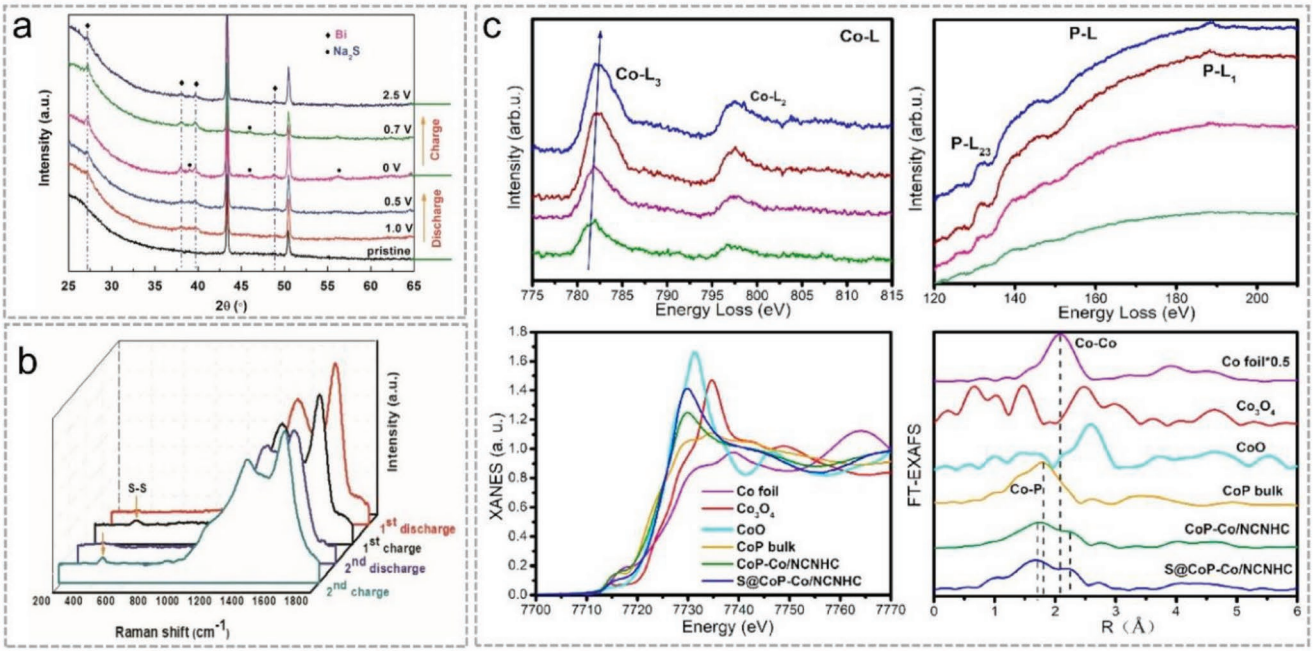

Figure 16. a) Ex situ XRD patterns of the Bi_2S_3 electrode charged or discharged to different states. Reproduced with permission.[131] Copyright 2016, Wiley-VCH. b) Ex situ Raman study of the sulfur cathode at fully discharged and charged states of the first and second cycles. Reproduced with permission.[72] Copyright 2020, Wiley-VCH. c) EXAFS characterization of the heterostructure of the CoP-Co composite. Reproduced with permission.[105] Copyright 2020, American Chemical Society.

functional separators. In this review, the latest developments on non-lithium MSBs have been systematically summarized in terms of the rational design of battery materials and components to enhance their electrochemical performance. Among different non-lithium MSBs, Na–S batteries would be the most promising candidate for replacing the conventional Li–S owing to the low price and abundance of Na reservoir. Compared with Na–S batteries, K–S batteries show a lower discharge capacity and energy density due to the sluggish reaction kinetics. In addition, K metal is more active than Na, causing severe safety concerns. For multivalent MSBs, the study is still in its infancy. Various critical challenges need to be addressed to promote the commercialization of non-lithium MSBs. Future research directions are proposed with the aid of experimental, theoretical, and computational capabilities for the advancement of non-lithium MSBs, as outlined below.

(1) To prevent the shuttling of polysulfides, the rational design of cathode hosts is the most frequently adopted approach. Similar to Li–S batteries, highly conductive carbon matrices, such as graphene, CNTs, and CNFs decorated with polar inorganic components, such as metal clusters, metal oxides, metal sulfides, metal nitrides, and MXenes are selected as sulfur hosts. In such a design, carbonaceous materials with various architectures (e.g., hollow, porous, yolk-shell, core-shell, etc.) allow the physical confinement of polysulfides and boost electron transfer, whereas polar components chemically adsorb the soluble polysulfide intermediates and promote the conversion reactions of sulfur. The synergy between carbon materials and polar species can suppress the shuttle effects of polysulfides, resulting in a much better electrochemical performance. Notably, the sulfur content in hosts should be well optimized because the area capacity of the sulfur cathode is determined by the sulfur content and utilization. Therefore, high sulfur content and utilization should be achieved to increase the energy density of MSBs. In this regard, the sulfur host should have a high pore volume and high electronic conductivity with a low mass. The integration of polar components that can catalyze the conversion of sulfur and polysulfides to the carbon matrix is desired to accelerate redox reactions. More importantly, facile and large-scale synthesis methods with good consistency should be developed.

(2) New electrolyte systems, especially for multivalent MSBs, should be carefully explored. As mentioned, multivalent metals are not compatible with conventional electrolytes used in alkali MSBs; therefore, the exploration of compatible and cheap electrolytes that facilitate reversible metal deposition and fast ion transfer is crucial for multivalent MSBs. Metal salts dissolved in RT ILs are widely adopted in Mg/Al–S batteries; however, the high viscosity and costs hinder the practical applications. Recently, all-solid-state electrolytes have been developed for Li–S batteries to eliminate polysulfide dissolution, but the reaction kinetics are still poor owing to the large contact resistance and the slow ionic diffusion in solid-phase reactants. In this context, further research should pay more attention to the exploitation of new electrolytes and additives.

(3) The formation of metal dendrites and their reactions with polysulfides deserve more attention. In non-lithium MSBs, metal dendrites would be certainly generated during reiterative plating/stripping processes, which greatly hinder the stability, durability, and safety of MSBs. Meanwhile, the

crosstalk of polysulfides in the battery makes the situation more complicated. The soluble polysulfides would be reduced on the metal anode, which not only removes sulfur capacity on the cathode but builds up highly resistive layers that passivate the metal anodes. Therefore, substantial efforts are needed to attain a sufficient level of performance for metal anodes to be used in non-lithium MSBs. For example, optimizing electrolyte formulas, constructing composite metal anodes, and building artificial SEIs can improve the stability and reversibility of metal anodes to a large extent.[210,211] With respect to multivalent metals, the careful design of appropriate electrolytes that render a passivation-free surface and reversible operation need more attempts. Moreover, other battery components, including separators, interlayers, and binders, need to be further optimized to improve the inhibition of polysulfide shuttling.

(4) The differences between non-lithium MSBs and Li–S batteries remain elusive and need to be further explored. For example, it has been recognized that even with a small amount of active contaminants, a compact passivation film is formed on multivalent metals, which renders the anode useless owing to its insulating characteristics and consequently results in large impedance, unlike alkali metals. Compared with Li/Na–S batteries, the reaction mechanisms of multivalent MSBs are still ambiguous because of the complex reactions between sulfur and metals as well as the complex structures of electrolytes. To this end, advanced in situ/ex situ characterization techniques and computational simulations should be combined to elucidate the fundamental mechanisms. Theoretical studies, including ab initio MD and DFT calculations, are powerful tools for correlating the computational results with experimental findings. They can offer new insights into battery performance and help to optimize the design of novel electrode materials.

(5) For practical applications, several important parameters including the E/S weight ratio, sulfur content, areal sulfur loading, negative/positive capacity ratio, CE, and testing protocols should be carefully evaluated. The energy density of non-lithium MSBs depends largely on the sulfur loading and sulfur utilization in the cathodes. Regarding the low electrical conductivity of sulfur, the rational design of sulfur composites with a high sulfur content and excellent electrically conductive network is of great importance to obtain high energy density. Meanwhile, the non-active components such as the binder, the conductive agent, and the current collector need to be investigated and optimized to realize high sulfur loading and respectable sulfur utilization. All the while, the E/S ratio also strongly affects the performance of batteries. In most current studies, this crucial parameter for non-lithium MSBs is often ignored. Without a means of decreasing the E/S ratio, the non-lithium MSBs are unlikely to compete with the current LIBs and lithium metal batteries with a conventional cathode in terms of gravimetric energy density. Therefore, we encourage future publications to specify these metrics to inform and direct future research efforts. For example, Muldoon et al. calculated that a prototype Li–S battery requires a sulfur loading of >3 mg cm^{-2}, an E/S ratio <3, and a sulfur utilization >75% to deliver 400 Wh kg^{-1}.[212] Therefore, for non-lithium MSBs, similar requirements should be fulfilled to highlight their competitiveness and commercial visibility. In terms of negative/positive capacity ratio, the amount of metal anode should be controlled without compromising the energy density of non-lithium MSBs. Currently, non-lithium MSBs are normally operated with excessive metal anodes to avoid exacerbating the challenges. However, in such a manner, the energy density of the battery will decrease dramatically. Therefore, improving the stability and reversibility of metal anodes is another intractable issue to be resolved to allow the use of an excess-free or a limited excess metal anode without penalizing cell performance. Currently, the vast majority of research on non-lithium MSBs is based on the testing of coin cells. Considering the increase in battery size and safety concerns for practical applications, practical pouch-type cells should be designed and tested in detail.

In summary, non-lithium MSBs have attracted increasing attention in the energy storage field. Although impressive progress has been made in the past several years, the development of non-lithium MSBs is still not mature enough to meet the practical requirements. Therefore, more experimental and theoretical studies are urgently required. Given the rapid development of sulfur cathodes, anodes, separators, and electrolytes, commercial applications of non-lithium MSBs will be expected in the near future.

Acknowledgements

This project was financially supported by the National Key Research and Development Program of China (2017YFA0208200), the Natural Science Foundation of China (22005003, 22022505, 21872069), the Fundamental Research Funds for the Central Universities of China (0205-14380219, 0205–14913212), the Scientific Research Foundation of Anhui University of Technology for Talent Introduction (DT19100069), the Yong Scientific Research Foundation of Anhui University of Technology (QZ202003), the Natural Science Foundation of Jiangsu Province (BK20180008), and the Shenzhen Fundamental Research Program of Science, Technology and Innovation Commission of Shenzhen Municipality (JCYJ20180307155007589).

Conflict of Interest

The authors declare no conflict of interest.

Keywords

advanced characterization techniques, electrolytes, non-lithium metal–sulfur batteries, separators, sulfur cathodes

Received: March 5, 2021
Revised: April 7, 2021
Published online: May 5, 2021

[1] J. M. Tarascon, M. Armand, *Nature* **2001**, *414*, 359.
[2] M. Armand, J. M. Tarascon, *Nature* **2008**, *451*, 652.
[3] J. B. Goodenough, K.-S. Park, *J. Am. Chem. Soc.* **2013**, *135*, 1167.
[4] Z. Yi, G. Chen, F. Hou, L. Wang, J. Liang, *Adv. Energy Mater.* **2021**, *11*, 2003065.

[5] V. Etacheri, R. Marom, R. Elazari, G. Salitra, D. Aurbach, *Energy Environ. Sci.* **2011**, *4*, 3243.
[6] N. Nitta, F. Wu, J. T. Lee, G. Yushin, *Mater. Today* **2015**, *18*, 252.
[7] P. G. Bruce, S. A. Freunberger, L. J. Hardwick, J.-M. Tarascon, *Nat. Mater.* **2012**, *11*, 19.
[8] X. Ji, K. T. Lee, L. F. Nazar, *Nat. Mater.* **2009**, *8*, 500.
[9] A. Manthiram, Y. Fu, S.-H. Chung, C. Zu, Y.-S. Su, *Chem. Rev.* **2014**, *114*, 11751.
[10] X. Hong, R. Wang, Y. Liu, J. Fu, J. Liang, S. Dou, *J. Energy Chem.* **2020**, *42*, 144.
[11] Y.-X. Yin, S. Xin, Y.-G. Guo, L.-J. Wan, *Angew. Chem., Int. Ed.* **2013**, *52*, 13186.
[12] A. Manthiram, Y. Fu, Y.-S. Su, *Acc. Chem. Res.* **2013**, *46*, 1125.
[13] Y. Yang, G. Zheng, Y. Cui, *Chem. Soc. Rev.* **2013**, *42*, 3018.
[14] X. Liang, C. Hart, Q. Pang, A. Garsuch, T. Weiss, L. F. Nazar, *Nat. Commun.* **2015**, *6*, 5682.
[15] S. Xin, L. Gu, N.-H. Zhao, Y.-X. Yin, L.-J. Zhou, Y.-G. Guo, L.-J. Wan, *J. Am. Chem. Soc.* **2012**, *134*, 18510.
[16] Z. W. Seh, Y. Sun, Q. Zhang, Y. Cui, *Chem. Soc. Rev.* **2016**, *45*, 5605.
[17] J. Mei, T. Liao, J. Liang, Y. Qiao, S. X. Dou, Z. Sun, *Adv. Energy Mater.* **2020**, *10*, 1901997.
[18] Z. Sang, X. Yan, D. Su, H. Ji, S. Wang, S. X. Dou, J. Liang, *Small* **2020**, *16*, 2001265.
[19] Y. Boyjoo, H. Shi, Q. Tian, S. Liu, J. Liang, Z.-S. Wu, M. Jaroniec, J. Liu, *Energy Environ. Sci.* **2021**, *14*, 540.
[20] H. Kim, G. Jeong, Y.-U. Kim, J.-H. Kim, C.-M. Park, H.-J. Sohn, *Chem. Soc. Rev.* **2013**, *42*, 9011.
[21] H.-J. Peng, J.-Q. Huang, Q. Zhang, *Chem. Soc. Rev.* **2017**, *46*, 5237.
[22] A. Manthiram, X. Yu, *Small* **2015**, *11*, 2108.
[23] X. Yuan, B. Zhu, J. Feng, C. Wang, X. Cai, K. Qiao, R. Qin, *Small* **2020**, *16*, 2003386.
[24] L. Kong, C. Yan, J.-Q. Huang, M.-Q. Zhao, M.-M. Titirici, R. Xiang, Q. Zhang, *Energy Environ. Mater.* **2018**, *1*, 100.
[25] A. Ponrouch, C. Frontera, F. Bardé, M. R. Palacín, *Nat. Mater.* **2016**, *15*, 169.
[26] Y. Wang, D. Zhou, V. Palomares, D. Shanmukaraj, B. Sun, X. Tang, C. Wang, M. Armand, T. Rojo, G. Wang, *Energy Environ. Sci.* **2020**, *13*, 3848.
[27] J. Ding, H. Zhang, W. Fan, C. Zhong, W. Hu, D. Mitlin, *Adv. Mater.* **2020**, *32*, 1908007.
[28] P. Wang, M. R. Buchmeiser, *Adv. Funct. Mater.* **2019**, *29*, 1905248.
[29] M. Salama, R. A. Rosy, R. Yemini, Y. Gofer, D. Aurbach, M. Noked, *ACS Energy Lett.* **2019**, *4*, 436.
[30] J. Wu, J. Liu, Z. Lu, K. Lin, Y.-Q. Lyu, B. Li, F. Ciucci, J.-K. Kim, *Energy Storage Mater.* **2019**, *23*, 8.
[31] X. Xu, D. Zhou, X. Qin, K. Lin, F. Kang, B. Li, D. Shanmukaraj, T. Rojo, M. Armand, G. Wang, *Nat. Commun.* **2018**, *9*, 3870.
[32] D. Zhou, Y. Chen, B. Li, H. Fan, F. Cheng, D. Shanmukaraj, T. Rojo, M. Armand, G. Wang, *Angew. Chem., Int. Ed.* **2018**, *57*, 10168.
[33] P. Mu, T. Dong, H. Jiang, M. Jiang, Z. Chen, H. Xu, H. Zhang, G. Cui, *Energy Fuels* **2021**, *35*, 1966.
[34] J. Luo, X. Lu, E. Matios, C. Wang, H. Wang, Y. Zhang, X. Hu, W. Li, *Nano Lett.* **2020**, *20*, 7700.
[35] J. Wu, P. Zou, M. Ihsan-Ul-Haq, N. Mubarak, A. Susca, B. Li, F. Ciucci, J.-K. Kim, *Small* **2020**, *16*, 2003815.
[36] H. Wang, E. Matios, J. Luo, W. Li, *Chem. Soc. Rev.* **2020**, *49*, 3783.
[37] D. Zhou, X. Tang, X. Guo, P. Li, D. Shanmukaraj, H. Liu, X. Gao, Y. Wang, T. Rojo, M. Armand, G. Wang, *Angew. Chem., Int. Ed.* **2020**, *59*, 16725.
[38] S. H. Chung, A. Manthiram, *Adv. Mater.* **2019**, *31*, 1901125.
[39] X. Hong, J. Mei, L. Wen, Y. Tong, A. J. Vasileff, L. Wang, J. Liang, Z. Sun, S. X. Dou, *Adv. Mater.* **2019**, *31*, 1802822.
[40] R. Steunenberg, C. Trapp, R. Yonco, E. Cairns, *Adv. Chem.* **1972**, *14*, 190.
[41] J. Zhu, J. Zou, H. Cheng, Y. Gu, Z. Lu, *Green Energy Environ.* **2019**, *4*, 345.
[42] F. Wu, C. Zhao, S. Chen, Y. Lu, Y. Hou, Y.-S. Hu, J. Maier, Y. Yu, *Mater. Today* **2018**, *21*, 960.
[43] L. He, Y.-R. Sun, C.-L. Wang, H.-Y. Guo, Y.-Q. Guo, C. Li, Y. Zhou, *New Carbon Mater* **2020**, *35*, 420.
[44] N. Chawla, M. Safa, *Electronics* **2019**, *8*, 1201.
[45] H. Tian, J. Liang, J. Liu, *Adv. Mater.* **2019**, *31*, 1903886.
[46] A. Y. S. Eng, D.-T. Nguyen, V. Kumar, G. S. Subramanian, M.-F. Ng, Z. W. Seh, *J. Mater. Chem. A* **2020**, *8*, 22983.
[47] J. Zhang, G. Zhang, Z. Chen, H. Dai, Q. Hu, S. Liao, S. Sun, *Energy Storage Mater.* **2020**, *26*, 513.
[48] Y.-X. Wang, W.-H. Lai, S.-L. Chou, H.-K. Liu, S.-X. Dou, *Adv. Mater.* **2020**, *32*, 1903952.
[49] T. Gao, S. Hou, K. Huynh, F. Wang, N. Eidson, X. Fan, F. Han, C. Luo, M. Mao, X. Li, C. Wang, *ACS Appl. Mater. Interfaces* **2018**, *10*, 14767.
[50] M. Rashad, M. Asif, Z. Ali, *Coord. Chem. Rev.* **2020**, *415*, 213312.
[51] B. Lee, E. Paek, D. Mitlin, S. W. Lee, *Chem. Rev.* **2019**, *119*, 5416.
[52] C. Wei, Y. Tao, H. Fei, Y. An, Y. Tian, J. Feng, Y. Qian, *Energy Storage Mater.* **2020**, *30*, 206.
[53] X. Lu, G. Li, J. Y. Kim, D. Mei, J. P. Lemmon, V. L. Sprenkle, J. Liu, *Nat. Commun.* **2014**, *5*, 4578.
[54] Y. Wang, Y. Hao, L.-C. Xu, Z. Yang, M.-Y. Di, R. Liu, X. Li, *J. Phys. Chem. C* **2019**, *123*, 3988.
[55] K. B. Hueso, M. Armand, T. Rojo, *Energy Environ. Sci.* **2013**, *6*, 734.
[56] Y. Yung-Fang Yu, J. T. Kummer, *J. Inorg. Nucl. Chem.* **1967**, *29*, 2453.
[57] A. K. Geim, K. S. Novoselov, *Nat. Mater.* **2007**, *6*, 183.
[58] A. H. Castro Neto, F. Guinea, N. M. R. Peres, K. S. Novoselov, A. K. Geim, *Rev. Mod. Phys.* **2009**, *81*, 109.
[59] Y. Hao, X. Li, X. Sun, C. Wang, *ChemistrySelect* **2017**, *2*, 9425.
[60] A. Ghosh, A. Kumar, A. Roy, M. R. Panda, M. Kar, D. R. MacFarlane, S. Mitra, *ACS Appl. Mater. Interfaces* **2019**, *11*, 14101.
[61] R. Singhal, S.-H. Chung, A. Manthiram, V. Kalra, *J. Mater. Chem. A* **2015**, *3*, 4530.
[62] Y. Zhang, G. Xu, Q. Kang, L. Zhan, W. Tang, Y. Yu, K. Shen, H. Wang, X. Chu, J. Wang, S. Zhao, Y. Wang, L. Ling, S. Yang, *J. Mater. Chem. A* **2019**, *7*, 16812.
[63] Q. Lu, X. Wang, J. Cao, C. Chen, K. Chen, Z. Zhao, Z. Niu, J. Chen, *Energy Storage Mater.* **2017**, *8*, 77.
[64] T. Zhu, X. Dong, Y. Liu, Y.-G. Wang, C. Wang, Y.-Y. Xia, *ACS Appl. Energy Mater.* **2019**, *2*, 5263.
[65] L. Zeng, Y. Yao, J. Shi, Y. Jiang, W. Li, L. Gu, Y. Yu, *Energy Storage Mater.* **2016**, *5*, 50.
[66] Y. Yao, L. Zeng, S. Hu, Y. Jiang, B. Yuan, Y. Yu, *Small* **2017**, *13*, 1603513.
[67] S. Wei, S. Xu, A. Agrawral, S. Choudhury, Y. Lu, Z. Tu, L. Ma, L. A. Archer, *Nat. Commun.* **2016**, *7*, 11722.
[68] Y.-M. Chen, W. Liang, S. Li, F. Zou, S. M. Bhaway, Z. Qiang, M. Gao, B. D. Vogt, Y. Zhu, *J. Mater. Chem. A* **2016**, *4*, 12471.
[69] H. Li, M. Zhao, B. Jin, Z. Wen, H. K. Liu, Q. Jiang, *Small* **2020**, *16*, 1907464.
[70] J. W. Jeon, D.-M. Kim, J. Lee, J.-C. Lee, Y. S. Kim, K. T. Lee, B. G. Kim, *J. Mater. Chem. A* **2020**, *8*, 3580.
[71] W. Du, Q. Xu, R. Zhan, Y. Zhang, Y. Luo, M. Xu, *Mater. Lett.* **2018**, *221*, 66.
[72] F. Xiao, X. Yang, H. Wang, J. Xu, Y. Liu, D. Y. W. Yu, A. L. Rogach, *Adv. Energy Mater.* **2020**, *10*, 2000931.
[73] L. Medenbach, I. Escher, N. Köwitsch, M. Armbrüster, L. Zedler, B. Dietzek, P. Adelhelm, *Angew. Chem., Int. Ed.* **2018**, *57*, 13666.
[74] J. Pampel, S. Dörfler, H. Althues, S. Kaskel, *Energy Storage Mater.* **2019**, *21*, 41.
[75] Y.-X. Wang, J. Yang, W. Lai, S.-L. Chou, Q.-F. Gu, H. K. Liu, D. Zhao, S. X. Dou, *J. Am. Chem. Soc.* **2016**, *138*, 16576.

[76] L. Hu, Y. Lu, T. Zhang, T. Huang, Y. Zhu, Y. Qian, *ACS Appl. Mater. Interfaces* **2017**, *9*, 13813.
[77] Z. Qiang, Y.-M. Chen, Y. Xia, W. Liang, Y. Zhu, B. D. Vogt, *Nano Energy* **2017**, *32*, 59.
[78] D.-J. Lee, J.-W. Park, I. Hasa, Y.-K. Sun, B. Scrosati, J. Hassoun, *J. Mater. Chem. A* **2013**, *1*, 5256.
[79] L. Zhang, B. Zhang, Y. Dou, Y. Wang, M. Al-Mamun, X. Hu, H. Liu, *ACS Appl. Mater. Interfaces* **2018**, *10*, 20422.
[80] R. Carter, L. Oakes, A. Douglas, N. Muralidharan, A. P. Cohn, C. L. Pint, *Nano Lett.* **2017**, *17*, 1863.
[81] Q. Guo, S. Li, X. Liu, H. Lu, X. Chang, H. Zhang, X. Zhu, Q. Xia, C. Yan, H. Xia, *Adv. Sci.* **2020**, *7*, 1903246.
[82] C. Luo, Y. Zhu, O. Borodin, T. Gao, X. Fan, Y. Xu, K. Xu, C. Wang, *Adv. Funct. Mater.* **2016**, *26*, 745.
[83] L. Fan, R. Ma, Y. Yang, S. Chen, B. Lu, *Nano Energy* **2016**, *28*, 304.
[84] K. Chen, H. Li, Y. Xu, K. Liu, H. Li, X. Xu, X. Qiu, M. Liu, *Nanoscale* **2019**, *11*, 5967.
[85] J. Yan, W. Li, R. Wang, P. Feng, M. Jiang, J. Han, S. Cao, Z. Zhang, K. Wang, K. Jiang, *ACS Energy Lett.* **2020**, *5*, 1307.
[86] S. Xin, Y.-X. Yin, Y.-G. Guo, L.-J. Wan, *Adv. Mater.* **2014**, *26*, 1261.
[87] G. Xia, L. Zhang, X. Chen, Y. Huang, D. Sun, F. Fang, Z. Guo, X. Yu, *Energy Storage Mater.* **2018**, *14*, 314.
[88] B.-W. Zhang, Y.-D. Liu, Y.-X. Wang, L. Zhang, M.-Z. Chen, W.-H. Lai, S.-L. Chou, H.-K. Liu, S.-X. Dou, *ACS Appl. Mater. Interfaces* **2017**, *9*, 24446.
[89] B.-W. Zhang, T. Sheng, Y.-X. Wang, S. Chou, K. Davey, S.-X. Dou, S.-Z. Qiao, *Angew. Chem., Int. Ed.* **2019**, *58*, 1484.
[90] M. K. Aslam, I. D. Seymour, N. Katyal, S. Li, T. Yang, S.-J. Bao, G. Henkelman, M. Xu, *Nat. Commun.* **2020**, *11*, 5242.
[91] B.-W. Zhang, T. Sheng, Y.-D. Liu, Y.-X. Wang, L. Zhang, W.-H. Lai, L. Wang, J. Yang, Q.-F. Gu, S.-L. Chou, H.-K. Liu, S.-X. Dou, *Nat. Commun.* **2018**, *9*, 4082.
[92] B. Guo, W. Du, T. Yang, J. Deng, D. Liu, Y. Qi, J. Jiang, S.-J. Bao, M. Xu, *Adv. Sci.* **2020**, *7*, 1902617.
[93] Q. Ma, G. Du, B. Guo, W. Tang, Y. Li, M. Xu, C. Li, *Chem. Eng. J.* **2020**, *388*, 124210.
[94] W. Du, W. Gao, T. Yang, B. Guo, L. Zhang, S.-J. Bao, Y. Chen, M. Xu, *J. Colloid Interface Sci.* **2020**, *565*, 63.
[95] N. Wang, Y. Wang, Z. Bai, Z. Fang, X. Zhang, Z. Xu, Y. Ding, X. Xu, Y. Du, S. Dou, G. Yu, *Energy Environ. Sci.* **2020**, *13*, 562.
[96] D. Ma, Y. Li, J. Yang, H. Mi, S. Luo, L. Deng, C. Yan, M. Rauf, P. Zhang, X. Sun, X. Ren, J. Li, H. Zhang, *Adv. Funct. Mater.* **2018**, *28*, 1705537.
[97] W. Du, Y. Wu, T. Yang, B. Guo, D. Liu, S.-J. Bao, M. Xu, *Chem. Eng. J.* **2020**, *379*, 122359.
[98] T. Yang, B. Guo, W. Du, M. K. Aslam, M. Tao, W. Zhong, Y. Chen, S.-J. Bao, X. Zhang, M. Xu, *Adv. Sci.* **2019**, *6*, 1901557.
[99] Z. Yan, J. Xiao, W. Lai, L. Wang, F. Gebert, Y. Wang, Q. Gu, H. Liu, S.-L. Chou, H. Liu, S.-X. Dou, *Nat. Commun.* **2019**, *10*, 4793.
[100] H. Wan, W. Weng, F. Han, L. Cai, C. Wang, X. Yao, *Nano Today* **2020**, *33*, 100860.
[101] R. K. Bhardwaj, S. Jayanthi, P. S. Adarakatti, A. K. Sood, A. J. Bhattacharyya, *ACS Appl. Mater. Interfaces* **2020**, *12*, 28120.
[102] H. Liu, W. Pei, W.-H. Lai, Z. Yan, H. Yang, Y. Lei, Y.-X. Wang, Q. Gu, S. Zhou, S. Chou, H. K. Liu, S. X. Dou, *ACS Nano* **2020**, *14*, 7259.
[103] G. Qin, Y. Liu, P. Han, S. Cao, X. Guo, Z. Guo, *Chem. Eng. J.* **2020**, *396*, 125295.
[104] W. Tang, W. Zhong, Y. Wu, Y. Qi, B. Guo, D. Liu, S.-J. Bao, M. Xu, *Chem. Eng. J.* **2020**, *395*, 124978.
[105] Z. Yan, Y. Liang, W. Hua, X.-G. Zhang, W. Lai, Z. Hu, W. Wang, J. Peng, S. Indris, Y. Wang, S.-L. Chou, H. Liu, S.-X. Dou, *ACS Nano* **2020**, *14*, 10284.
[106] A. Ghosh, A. Kumar, T. Das, A. Ghosh, S. Chakraborty, M. Kar, D. R. MacFarlane, S. Mitra, *Adv. Funct. Mater.* **2020**, *30*, 2005669.
[107] W. Bao, C. E. Shuck, W. Zhang, X. Guo, Y. Gogotsi, G. Wang, *ACS Nano* **2019**, *13*, 11500.
[108] X. Huo, Y. Liu, R. Li, J. Li, *Ionics* **2019**, *25*, 5373.
[109] C. Ye, Y. Jiao, D. Chao, T. Ling, J. Shan, B. Zhang, Q. Gu, K. Davey, H. Wang, S.-Z. Qiao, *Adv. Mater.* **2020**, *32*, 1907557.
[110] W. H. Lai, H. Wang, L. Zheng, Q. Jiang, Z. C. Yan, L. Wang, H. Yoshikawa, D. Matsumura, Q. Sun, Y. X. Wang, Q. Gu, J.-Z. Wang, H.-K. Liu, S.-L. Chou, S.-X. Dou, *Angew. Chem., Int. Ed.* **2020**, *59*, 22171.
[111] X. Fan, J. Yue, F. Han, J. Chen, T. Deng, X. Zhou, S. Hou, C. Wang, *ACS Nano* **2018**, *12*, 3360.
[112] L. M. Bloi, J. Pampel, S. Dörfler, H. Althues, S. Kaskel, *Adv. Energy Mater.* **2020**, *10*, 1903245.
[113] C. Wang, H. Wang, X. Hu, E. Matios, J. Luo, Y. Zhang, X. Lu, W. Li, *Adv. Energy Mater.* **2019**, *9*, 1803251.
[114] X. Yu, A. Manthiram, *J. Phys. Chem. C* **2014**, *118*, 22952.
[115] X. Yu, A. Manthiram, *Chem. Mater.* **2016**, *28*, 896.
[116] X. Yu, A. Manthiram, *Chem. - Eur. J.* **2015**, *21*, 4233.
[117] A. Kumar, A. Ghosh, M. Forsyth, D. R. MacFarlane, S. Mitra, *ACS Energy Lett.* **2020**, *5*, 2112.
[118] X. Yu, A. Manthiram, *Adv. Energy Mater.* **2015**, *5*, 1500350.
[119] A. Kumar, A. Ghosh, A. Roy, M. R. Panda, M. Forsyth, D. R. MacFarlane, S. Mitra, *Energy Storage Mater.* **2019**, *20*, 196.
[120] N. Tanibata, H. Tsukasaki, M. Deguchi, S. Mori, A. Hayashi, M. Tatsumisago, *Solid State Ionics* **2017**, *311*, 6.
[121] S. Wei, L. Ma, K. E. Hendrickson, Z. Tu, L. A. Archer, *J. Am. Chem. Soc.* **2015**, *137*, 12143.
[122] S. Li, Z. Zeng, J. Yang, Z. Han, W. Hu, L. Wang, J. Ma, B. Shan, J. Xie, *ACS Appl. Energy Mater.* **2019**, *2*, 2956.
[123] I. Kim, C. H. Kim, S. h. Choi, J.-P. Ahn, J.-H. Ahn, K.-W. Kim, E. J. Cairns, H.-J. Ahn, *J. Power Sources* **2016**, *307*, 31.
[124] L. Wang, X. Chen, S. Li, J. Yang, Y. Sun, L. Peng, B. Shan, J. Xie, *J. Mater. Chem. A* **2019**, *7*, 12732.
[125] S. Ma, P. Zuo, H. Zhang, Z. Yu, C. Cui, M. He, G. Yin, *Chem. Commun.* **2019**, *55*, 5267.
[126] J. Wang, J. Yang, Y. Nuli, R. Holze, *Electrochem. Commun.* **2007**, *9*, 31.
[127] T. H. Hwang, D. S. Jung, J.-S. Kim, B. G. Kim, J. W. Choi, *Nano Lett.* **2013**, *13*, 4532.
[128] A. Ghosh, S. Shukla, M. Monisha, A. Kumar, B. Lochab, S. Mitra, *ACS Energy Lett.* **2017**, *2*, 2478.
[129] T. Wu, M. Jing, L. Yang, G. Zou, H. Hou, Y. Zhang, Y. Zhang, X. Cao, X. Ji, *Adv. Energy Mater.* **2019**, *9*, 1803478.
[130] M. L. Meyerson, P. E. Papa, J. A. Weeks, A. G. Paul-Orecchio, A. Heller, C. B. Mullins, *ACS Appl. Energy Mater.* **2020**, *3*, 6121.
[131] W.-J. Li, C. Han, S.-L. Chou, J.-Z. Wang, Z. Li, Y.-M. Kang, H.-K. Liu, S.-X. Dou, *Chem. - Eur. J.* **2016**, *22*, 590.
[132] A. Douglas, R. Carter, L. Oakes, K. Share, A. P. Cohn, C. L. Pint, *ACS Nano* **2015**, *9*, 11156.
[133] P. Li, L. Ma, T. Wu, H. Ye, J. Zhou, F. Zhao, N. Han, Y. Wang, Y. Wu, Y. Li, J. Lu, *Adv. Energy Mater.* **2018**, *8*, 1800624.
[134] T. Li, J. Xu, C. Wang, W. Wu, D. Su, G. Wang, *J. Alloys Compd.* **2019**, *792*, 797.
[135] X.-M. Zhao, Q. Zhu, S.-D. Xu, L. Chen, Z.-J. Zuo, X.-M. Wang, S.-B. Liu, D. Zhang, *J. Electroanal. Chem.* **2019**, *832*, 392.
[136] H. Ryu, T. Kim, K. Kim, J.-H. Ahn, T. Nam, G. Wang, H.-J. Ahn, *J. Power Sources* **2011**, *196*, 5186.
[137] D. Di Lecce, L. Minnetti, D. Polidoro, V. Marangon, J. Hassoun, *Ionics* **2019**, *25*, 3129.
[138] M. Kohl, F. Borrmann, H. Althues, S. Kaskel, *Adv. Energy Mater.* **2016**, *6*, 1502185.
[139] N. Tanibata, M. Deguchi, A. Hayashi, M. Tatsumisago, *Chem. Mater.* **2017**, *29*, 5232.
[140] K. Lu, B. Li, X. Zhan, F. Xia, O. J. Dahunsi, S. Gao, D. M. Reed, V. L. Sprenkle, G. Li, Y. Cheng, *Nano Lett.* **2020**, *20*, 6837.

[141] D. Kumar, D. K. Kanchan, *J. Energy Storage* **2019**, *22*, 44.
[142] G. Nikiforidis, G. J. Jongerden, E. F. Jongerden, M. C. M. van de Sanden, M. N. Tsampas, *J. Electrochem. Soc.* **2019**, *166*, A135.
[143] L. Fan, M. Li, X. Li, W. Xiao, Z. Chen, J. Lu, *Joule* **2019**, *3*, 361.
[144] Y. Peng, Y. Zhang, Y. Wang, X. Shen, F. Wang, H. Li, B.-J. Hwang, J. Zhao, *ACS Appl. Mater. Interfaces* **2017**, *9*, 29804.
[145] E. Ceylan Cengiz, Z. Erdol, B. Sakar, A. Aslan, A. Ata, O. Ozturk, R. Demir-Cakan, *J. Phys. Chem. C* **2017**, *121*, 15120.
[146] Y. X. Ren, H. R. Jiang, T. S. Zhao, L. Zeng, C. Xiong, *J. Power Sources* **2018**, *396*, 304.
[147] A. P. Vijaya Kumar Saroja, K. M, R. Sundara, *J. Phys. Chem. C* **2020**, *124*, 7615.
[148] I. Bauer, M. Kohl, H. Althues, S. Kaskel, *Chem. Commun.* **2014**, *50*, 3208.
[149] S. Lee, J. Lee, J. Kim, M. Agostini, S. Xiong, A. Matic, J.-Y. Hwang, *Energies* **2020**, *13*, 2791.
[150] Q. Zhao, Y. Hu, K. Zhang, J. Chen, *Inorg. Chem.* **2014**, *53*, 9000.
[151] P. Xiong, X. Han, X. Zhao, P. Bai, Y. Liu, J. Sun, Y. Xu, *ACS Nano* **2019**, *13*, 2536.
[152] J.-Y. Hwang, H. M. Kim, C. S. Yoon, Y.-K. Sun, *ACS Energy Lett.* **2018**, *3*, 540.
[153] X. Zhao, Y. Hong, M. Cheng, S. Wang, L. Zheng, J. Wang, Y. Xu, *J. Mater. Chem. A* **2020**, *8*, 10875.
[154] J.-Y. Hwang, H. M. Kim, Y.-K. Sun, *J. Mater. Chem. A* **2018**, *6*, 14587.
[155] Y. Liu, W. Wang, J. Wang, Y. Zhang, Y. Zhu, Y. Chen, L. Fu, Y. Wu, *Chem. Commun.* **2018**, *54*, 2288.
[156] Y. Zhang, J. Lou, Y. Shuai, K. Chen, X. He, Y. Wang, N. Li, Z. Zhang, F. Gan, *Mater. Lett.* **2019**, *242*, 5.
[157] N.-C. Lai, G. Cong, Y.-C. Lu, *J. Mater. Chem. A* **2019**, *7*, 20584.
[158] L. Wang, J. Bao, Q. Liu, C.-F. Sun, *Energy Storage Mater.* **2019**, *18*, 470.
[159] X. Lu, M. E. Bowden, V. L. Sprenkle, J. Liu, *Adv. Mater.* **2015**, *27*, 5915.
[160] Z. Meng, D. Foix, N. Brun, R. Dedryvère, L. Stievano, M. Morcrette, R. Berthelot, *ACS Energy Lett.* **2019**, *4*, 2040.
[161] Z. Zhou, B. Chen, T. Fang, Y. Li, Z. Zhou, Q. Wang, J. Zhang, Y. Zhao, *Adv. Energy Mater.* **2020**, *10*, 1902023.
[162] H. O. Ford, L. C. Merrill, P. He, S. P. Upadhyay, J. L. Schaefer, *Macromolecules* **2018**, *51*, 8629.
[163] B. P. Vinayan, Z. Zhao-Karger, T. Diemant, V. S. K. Chakravadhanula, N. I. Schwarzburger, M. A. Cambaz, R. J. Behm, C. Kübel, M. Fichtner, *Nanoscale* **2016**, *8*, 3296.
[164] H. Du, Z. Zhang, J. He, Z. Cui, J. Chai, J. Ma, Z. Yang, C. Huang, G. Cui, *Small* **2017**, *13*, 1702277.
[165] X. Yu, A. Manthiram, *ACS Energy Lett.* **2016**, *1*, 431.
[166] R. Richter, J. Häcker, Z. Zhao-Karger, T. Danner, N. Wagner, M. Fichtner, K. A. Friedrich, A. Latz, *ACS Appl. Energy Mater.* **2020**, *3*, 8457.
[167] W. Wang, H. Yuan, Y. NuLi, J. Zhou, J. Yang, J. Wang, *J. Phys. Chem. C* **2018**, *122*, 26764.
[168] J. Häcker, C. Danner, B. Sievert, I. Biswas, Z. Zhao-Karger, N. Wagner, K. A. Friedrich, *Electrochim. Acta* **2020**, *338*, 135787.
[169] J. Sun, C. Deng, Y. Bi, K.-H. Wu, S. Zhu, Z. Xie, C. Li, R. Amal, J. Luo, T. Liu, D.-W. Wang, *ACS Appl. Energy Mater.* **2020**, *3*, 2516.
[170] X. Zhou, J. Tian, J. Hu, C. Li, *Adv. Mater.* **2018**, *30*, 1704166.
[171] S. Zhang, Y. Huang, Y. NuLi, B. Wang, J. Yang, J. Wang, *J. Phys. Chem. C* **2020**, *124*, 20712.
[172] P. Wang, J. Kappler, B. Sievert, J. Häcker, K. Küster, U. Starke, F. Ziegler, M. R. Buchmeiser, *Electrochim. Acta* **2020**, *361*, 137024.
[173] P. Wang, J. Trück, S. Niesen, J. Kappler, K. Küster, U. Starke, F. Ziegler, A. Hintennach, M. R. Buchmeiser, *Batteries Supercaps* **2020**, *3*, 1239.
[174] A. Robba, A. Vizintin, J. Bitenc, G. Mali, I. Arčon, M. Kavčič, M. Žitnik, K. Bučar, G. Aquilanti, C. Martineau-Corcos, A. Randon-Vitanova, R. Dominko, *Chem. Mater.* **2017**, *29*, 9555.
[175] Y. Nakayama, R. Matsumoto, K. Kumagae, D. Mori, Y. Mizuno, S. Hosoi, K. Kamiguchi, N. Koshitani, Y. Inaba, Y. Kudo, H. Kawasaki, E. C. Miller, J. N. Weker, M. F. Toney, *Chem. Mater.* **2018**, *30*, 6318.
[176] H. S. Kim, T. S. Arthur, G. D. Allred, J. Zajicek, J. G. Newman, A. E. Rodnyansky, A. G. Oliver, W. C. Boggess, J. Muldoon, *Nat. Commun.* **2011**, *2*, 427.
[177] L. Zeng, N. Wang, J. Yang, J. Wang, Y. NuLi, *J. Electrochem. Soc.* **2017**, *164*, A2504.
[178] Z. Zhao-Karger, X. Zhao, D. Wang, T. Diemant, R. J. Behm, M. Fichtner, *Adv. Energy Mater.* **2015**, *5*, 1401155.
[179] Y. Xu, Y. Ye, S. Zhao, J. Feng, J. Li, H. Chen, A. Yang, F. Shi, L. Jia, Y. Wu, X. Yu, P.-A. Glans-Suzuki, Y. Cui, J. Guo, Y. Zhang, *Nano Lett.* **2019**, *19*, 2928.
[180] Y. Xu, W. Li, G. Zhou, Z. Pan, Y. Zhang, *Energy Storage Mater.* **2018**, *14*, 253.
[181] J. Wu, Z. Lu, K. Li, J. Cui, S. Yao, M. Ihsan-ul Haq, B. Li, Q.-H. Yang, F. Kang, F. Ciucci, J.-K. Kim, *J. Mater. Chem. A* **2018**, *6*, 5668.
[182] H. Fan, Y. Zhao, J. Xiao, J. Zhang, M. Wang, Y. Zhang, *Nano Res.* **2020**, *13*, 2749.
[183] A. Du, Z. Zhang, H. Qu, Z. Cui, L. Qiao, L. Wang, J. Chai, T. Lu, S. Dong, T. Dong, H. Xu, X. Zhou, G. Cui, *Energy Environ. Sci.* **2017**, *10*, 2616.
[184] W. Li, S. Cheng, J. Wang, Y. Qiu, Z. Zheng, H. Lin, S. Nanda, Q. Ma, Y. Xu, F. Ye, M. Liu, L. Zhou, Y. Zhang, *Angew. Chem., Int. Ed.* **2016**, *55*, 6406.
[185] Z. Zhao-Karger, R. Liu, W. Dai, Z. Li, T. Diemant, B. P. Vinayan, C. Bonatto Minella, X. Yu, A. Manthiram, R. J. Behm, M. Ruben, M. Fichtner, *ACS Energy Lett.* **2018**, *3*, 2005.
[186] Z. Zhang, Z. Cui, L. Qiao, J. Guan, H. Xu, X. Wang, P. Hu, H. Du, S. Li, X. Zhou, S. Dong, Z. Liu, G. Cui, L. Chen, *Adv. Energy Mater.* **2017**, *7*, 1602055.
[187] Y. Yang, W. Wang, Y. Nuli, J. Yang, J. Wang, *ACS Appl. Mater. Interfaces* **2019**, *11*, 9062.
[188] X. Zhao, Y. Yang, Y. NuLi, D. Li, Y. Wang, X. Xiang, *Chem. Commun.* **2019**, *55*, 6086.
[189] V. Bhaghavathi Parambath, Z. Zhao-Karger, T. Diemant, M. Jäckle, Z. Li, T. Scherer, A. Gross, R. J. Behm, M. Fichtner, *J. Mater. Chem. A* **2020**, *8*, 22998.
[190] H. Xu, Z. Zhang, J. Li, L. Qiao, C. Lu, K. Tang, S. Dong, J. Ma, Y. Liu, X. Zhou, G. Cui, *ACS Appl. Mater. Interfaces* **2018**, *10*, 23757.
[191] K. A. See, J. A. Gerbec, Y.-S. Jun, F. Wudl, G. D. Stucky, R. Seshadri, *Adv. Energy Mater.* **2013**, *3*, 1056.
[192] D. Aurbach, R. Skaletsky, Y. Gofer, *J. Electrochem. Soc.* **1991**, *138*, 3536.
[193] Z. Li, B. P. Vinayan, T. Diemant, R. J. Behm, M. Fichtner, Z. Zhao-Karger, *Small* **2020**, *16*, 2001806.
[194] A. Scafuri, R. Berthelot, K. Pirnat, A. Vizintin, J. Bitenc, G. Aquilanti, D. Foix, R. Dedryvère, I. Arčon, R. Dominko, L. Stievano, *Chem. Mater.* **2020**, *32*, 8266.
[195] X. Yu, M. J. Boyer, G. S. Hwang, A. Manthiram, *Adv. Energy Mater.* **2019**, *9*, 1803794.
[196] G. Cohn, L. Ma, L. A. Archer, *J. Power Sources* **2015**, *283*, 416.
[197] Y. Guo, H. Jin, Z. Qi, Z. Hu, H. Ji, L.-J. Wan, *Adv. Funct. Mater.* **2019**, *29*, 1807676.
[198] J. Smajic, S. Wee, F. R. F. Simoes, M. N. Hedhili, N. Wehbe, E. Abou-Hamad, P. M. F. J. Costa, *ACS Appl. Energy Mater.* **2020**, *3*, 6805.
[199] T. Gao, X. Li, X. Wang, J. Hu, F. Han, X. Fan, L. Suo, A. J. Pearse, S. B. Lee, G. W. Rubloff, K. J. Gaskell, M. Noked, C. Wang, *Angew. Chem., Int. Ed.* **2016**, *55*, 9898.
[200] W. Wang, Z. Cao, G. A. Elia, Y. Wu, W. Wahyudi, E. Abou-Hamad, A.-H. Emwas, L. Cavallo, L.-J. Li, J. Ming, *ACS Energy Lett.* **2018**, *3*, 2899.

[201] C. B. S. Sungjemmenla, V. Kumar, *Nanoscale Adv.* **2021**, *3*, 1569.
[202] X. Yu, A. Manthiram, *Adv. Energy Mater.* **2017**, *7*, 1700561.
[203] Y. Zhang, L. Ma, R. Tang, X. Zheng, X. Wang, Y. Dong, G. Kong, F. Zhao, L. Wei, *Int. J. Hydrogen Energy* **2021**, *46*, 4936.
[204] J. Lampkin, H. Li, L. Furness, R. Raccichini, N. Garcia-Araez, *ChemSusChem* **2020**, *13*, 3514.
[205] H. Yang, L. Yin, J. Liang, Z. Sun, Y. Wang, H. Li, K. He, L. Ma, Z. Peng, S. Qiu, C. Sun, H.-M. Cheng, F. Li, *Angew. Chem., Int. Ed.* **2018**, *57*, 1898.
[206] X. Yu, M. J. Boyer, G. S. Hwang, A. Manthiram, *Chem* **2018**, *4*, 586.
[207] Y. Bian, Y. Li, Z. Yu, H. Chen, K. Du, C. Qiu, G. Zhang, Z. Lv, M.-C. Lin, *ChemElectroChem* **2018**, *5*, 3607.
[208] Z. Hu, Y. Guo, H. Jin, H. Ji, L.-J. Wan, *Chem. Commun.* **2020**, *56*, 2023.
[209] W. Chu, X. Zhang, J. Wang, S. Zhao, S. Liu, H. Yu, *Energy Storage Mater.* **2019**, *22*, 418.
[210] L. Ma, J. Cui, S. Yao, X. Liu, Y. Luo, X. Shen, J.-K. Kim, *Energy Storage Mater.* **2020**, *27*, 522.
[211] L. Ma, J. Wu, G. Zhu, Y. Lv, Y. Zhang, H. Pang, *J. Mater. Chem. A* **2021**, *9*, 5232.
[212] P. Bonnick, J. Muldoon, *Energy Environ. Sci.* **2020**, *13*, 4808.

Lianbo Ma received his Ph.D. in Physical Chemistry from Nanjing University. Then, he got a Postdoc. position sponsored by the Hong Kong Innovation and Technology Fund (ITF), and worked at The Hong Kong University of Science and Technology (HKUST). In October 2019, he joined the School of Materials Science and Engineering at Anhui University of Technology. His research mainly includes the development of novel micro-nanostructured materials for secondary batteries, and the exploration of integrated energy conversion and storage devices.

Junxiong Wu received his M.S. from Tsinghua University, then he completed his Ph.D. in the Department of Mechanical and Aerospace Engineering at the Hong Kong University of Science and Technology (HKUST). Currently, he is the Postdoctoral Fellow at The Hong Kong Polytechnic University. His research mainly focuses on new materials for secondary batteries.

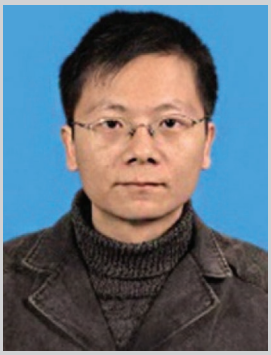

Zhong Jin received his B.S. degree and Ph.D. degree in Chemistry from Peking University in 2003 and 2008, respectively. Then, he pursued postdoctoral studies at Rice University (2008–2010) and MIT (2010–2014). Since 2014, he has been appointed as a professor at Nanjing University, China. His research is focusing on the nanostructural design, interfacial engineering, and mechanism studies of redox-active or redox-promoting electrode materials for clean energy conversion and storage device applications, such as secondary batteries, fuel cells, solar cells, and photocatalytic/electrocatalytic systems.